Constraints on the formation of carbonates and lowgrade metamorphic phases in the Martian crust as a function of H_2OCO_2 fluids

The Meteoritical Society

Meteoritics & Planetary Science 1–28 (2021)
doi: 10.1111/maps.13775

Constraints on the formation of carbonates and low-grade metamorphic phases in the Martian crust as a function of H_2O-CO_2 fluids

Julia SEMPRICH [1,2*], Justin FILIBERTO [2,3], Allan H. TREIMAN [2], and Susanne P. SCHWENZER [1]

[1]AstrobiologyOU, School of Environment, Earth and Ecosystem Sciences, The Open University, Walton Hall, Milton Keynes MK7 6AA, UK
[2]Lunar and Planetary Institute, USRA, 3600 Bay Area Blvd, Houston, Texas 77058, USA
[3]Astromaterials Research and Exploration Science (ARES) Division, XI3, NASA Johnson Space Center, Houston, Texas 77058, USA
[*]Corresponding author. E-mail: julia.semprich@open.ac.uk

(Received 11 August 2021; revision accepted 28 November 2021)

Abstract–Low-grade metamorphic hydrous minerals and carbonates occur in various settings on Mars and in Martian meteorites. We present constraints on the stability of prehnite, zeolites, serpentine, and carbonates by modeling the influence of H_2O-CO_2 fluids during low-grade metamorphism in the Martian crust using compositions of a Martian basalt and an ultramafic cumulate. In basaltic compositions with 5 wt% fluid, our models predict prehnite in less oxidized, CO_2-poor conditions (≤0.44 mol kg^{-1} CO_2) on warmer geotherms of 20 °C km^{-1}. At fluid-saturated conditions, epidote and laumontite are replaced by quartz, calcite, chlorite, and muscovite. In ultramafic compositions with 5 wt% fluid, antigorite (serpentine) is stable at CO_2-poor conditions of ≤0.33 mol kg^{-1}, while talc forms at 0.05–0.56 mol kg^{-1} CO_2. At fluid-saturated conditions, antigorite is replaced by talc and chlorite, and at higher $X(CO_2)$ by magnesite and quartz. Our models therefore suggest that prehnite, zeolites, and serpentine have formed in a CO_2-poor environment on Mars implying that fluids during their formation either did not contain high amounts of CO_2 or had degassed CO_2. Carbonates and potentially talc would have formed in the presence of a CO_2-bearing fluid and therefore at different alteration stages than for prehnite, zeolites, and serpentine either in the same hydrothermal event during which the fluid composition changed gradually due to cooling and precipitation or by separate and successive alteration events with fluids of different compositions.

INTRODUCTION

Carbonate minerals are of special interest in the study of the potential for life on Mars, since they are linked to both the water and inorganic carbon cycles (e.g., Niles et al., 2013). Locations where hydrated phyllosilicates and carbonates have been detected, such as in the Nili Fossae region as well as Leighton and McLaughlin craters, could be particularly suitable for a deep biosphere on Mars, as they suggest a prolonged past presence of alkaline water, carbon, and temperatures above freezing, all of which are critical prerequisites for life (Michalski & Niles, 2010; Michalski et al., 2013; Niles et al., 2013). The Martian subsurface may be a habitable environment for chemolithoautotrophic microorganisms since it is protected from surface radiation, provides increased porosity and permeability due to the lower gravity on Mars, includes possible nutrients and energy from geochemical sources such as serpentinization reactions (Fisk & Giovannoni, 1999; Jones et al., 2011; Michalski et al., 2013; Schrenk et al., 2013), and provides a habitable zone possibly extending up to 14 km below the surface (McMahon et al., 2013).

Better constraints on mineral stabilities and reactions in the Martian upper crust as a function of H_2O-CO_2 fluid variations are therefore critical to assess the habitability potential of the subsurface. In this study, we

use phase equilibria modeling to study the effect of fluid composition on low-grade metamorphic reactions.

While this study is focused on metamorphic subsurface fluids at temperatures above 150 °C, which is higher than the known limit of 122 °C (at elevated hydrostatic pressure) for the survival of terrestrial hyperthermophilic microbes (Takai et al., 2008), these initially hot fluids could cool down over geological timescales and circulate through the subsurface by geothermal gradient-driven groundwater convection (Travis et al., 2003).

Among the abundant alteration phases that have been detected on Mars from orbit (e.g., Bibring et al., 2006; Ehlmann & Edwards, 2014; Lasue et al., 2019; Mustard, 2019), at every landing site (e.g., Bristow et al., 2018; Jolliff et al., 2019; Kounaves & Oberlin, 2019; Mittlefehldt et al., 2019; Sutter et al., 2019; Rampe et al., 2020; Tu et al., 2021), and in Martian meteorites (e.g., Bridges et al., 2019; Filiberto et al., 2014; Giesting & Filiberto, 2016; McCubbin et al., 2013; Sautter et al., 2006), hydrous minerals such as prehnite, serpentine, epidote, and zeolites—spectrally observed from orbital measurements—are indicative of low-grade metamorphic conditions (Ehlmann et al., 2009, 2011; McSween et al., 2015; Viviano et al., 2013). Phase diagram and thermodynamic modeling studies suggest that these minerals formed at elevated temperatures (>150 °C) either along a normal geothermal gradient or as a result of impact- or volcanic-induced hydrothermal systems (McSween et al., 2015; Schwenzer & Kring, 2013; Semprich et al., 2019).

The physical conditions and water abundances required for the formation of OH-bearing low-grade metamorphic phases in Martian basaltic and ultramafic rock compositions have been investigated via phase equilibria modeling assuming the fluid to be pure H_2O (Semprich et al., 2019). The models estimated the formation of prehnite from basaltic protoliths to require at least 2.5 wt% water in the system. Serpentine forms by alteration of ultramafic compositions at >2.7 wt% H_2O (Semprich et al., 2019). While water is fundamental for the formation of these characteristic minerals, potential Martian subsurface fluids likely contain other species in addition to H_2O, such as CO_2 as suggested by the presence of carbonates detected on Mars and in meteorites (e.g., Bandfield et al., 2003; Bridges et al., 2019; Ehlmann, Mustard, Murchie, et al., 2008; Leshin et al., 2013; Morris et al., 2010; Sutter et al., 2012).

Carbonates have been identified on Mars in various settings (1) from orbit by remote sensing in dust (Bandfield et al., 2003) and associated with impact craters and canyons (e.g., Amador et al., 2018; Bishop et al., 2013; Brown et al., 2010; Carter & Poulet, 2012; Carter et al., 2015; Ehlmann, Mustard, Murchie, et al., 2008; Ehlmann et al., 2009; Jain & Chauhan, 2015; Michalski & Niles, 2010; Thomas & Bandfield, 2017; Wray et al., 2016); (2) in situ by the Phoenix lander, and Spirit and Curiosity rovers (Archer et al., 2020; Boynton et al., 2009; Morris et al., 2010; Stern et al., 2018; Sutter et al., 2012, 2017); and (3) in Martian meteorites, including ALH 84001 and the nakhlites (Bridges & Grady, 2000; Bridges et al., 2019; Changela & Bridges, 2011; Harvey & McSween, 1996; Hicks et al., 2014; Mittlefehldt, 1994). Importantly, carbonates are expected, based on orbital spectroscopic measurements, to be a dominant alteration phase in Jezero crater, the landing site of Mars 2020 Perseverance Rover (e.g., Brown et al., 2020; Goudge et al., 2015, 2017; Horgan et al., 2020; Salvatore et al., 2018). Carbonates reported by orbital spectral measurements mainly occur as layered-to-massive deposits in olivine-bearing Noachian regions (Ehlmann, Mustard, Murchie, et al., 2008) with abundances of up to ~20% (Edwards & Ehlmann, 2015) or as sedimentary deposits associated with Fe/Mg clays (Ehlmann, Mustard, Fassett, et al., 2008; Ehlmann et al., 2009). Deep crustal carbonate-bearing rocks may be present as suggested by their exposure in impact craters (e.g., Leighton crater) from depths of ~6 km (Michalski & Niles, 2010). Furthermore, the detection of Mg-carbonates associated with Mg-Fe-bearing clays in McLaughlin crater has been interpreted to result from upwelling of alkaline groundwater (Michalski et al., 2013). The majority of carbonates, therefore, seem to be locally restricted and likely formed by hydrothermal events with limited water availability primarily in the early to mid-Noachian rather than during an early dense atmosphere creating global warm and wet conditions with surficial water bodies (e.g., Bridges et al., 2019; Niles et al., 2013). Some carbonates formed as late as the Amazonian period as indicated by observations from orbit (Bultel et al., 2015; Turner et al., 2016) and by siderite in nakhlite meteorites (Bridges et al., 2019, and references therein).

Processes suggested for the crystallization of carbonates on Mars include (1) as a product of serpentinization (Amador et al., 2017; Brown et al., 2010, and references therein) although a study of spectral data across Mars only identified serpentine together with carbonates in the Nili Fossae region (Amador et al., 2018); (2) as an alteration product of either olivine or serpentine due to volcanic- or impact-related hydrothermal activity (Ehlmann, Mustard, Murchie, et al., 2008; Ehlmann et al., 2009; Golden et al., 2000; Viviano et al., 2013); (3) as sedimentary (fluvial/lacustrine/aeolian) detrital or in situ deposits (Doran et al., 1998; Goudge et al., 2015; Grotzinger et al., 2005; Horgan et al., 2020); (4) by diagenesis in a low-temperature environment (e.g., Van Berk & Fu, 2011); (5) by fluid evaporation (Boynton et al., 2009; Ruff et al., 2014); and (6) by weathering of olivine-rich

rocks exposed at the surface (Bultel et al., 2019). A combination of processes may also be feasible as suggested for the olivine–carbonate mineralogy in Jezero crater (Brown et al., 2020). The lack of widespread carbonate deposits on the Martian surface could also indicate that most alteration processes occurred in the subsurface not in contact with the atmosphere (e.g., Ehlmann et al., 2011). This is corroborated by carbonates being mixed with igneous minerals at Nili Fossae (Ehlmann, Mustard, Murchie, et al., 2008), Leighton crater (Michalski et al., 2013), and Gusev cater (Morris et al., 2010), suggesting their formation by fluid alteration in the subsurface rather than sedimentary processes (Niles et al., 2013). Furthermore, carbonates in meteorites were likely formed during brief subsurface aqueous events (Bridges & Schwenzer, 2012; Bridges et al., 2019; Changela & Bridges, 2011; Valley et al., 1997). Additionally, spectral features in thermal emission spectrometer (TES) data in northeast Syrtis Major and several other regions on Mars are best explained by the presence of carbonate decomposition products, which could indicate an interaction of lavas with subsurface carbonate deposits or devolatilization of initially carbonate-bearing lavas by later impacts of magmatic activity (Glotch & Rogers, 2013). Understanding the role of CO_2 in fluid–rock interaction models and its influence on low-grade metamorphic mineral stability and phase relations can therefore provide better constraints on subsurface fluid conditions.

Several thermochemical models have produced carbonates using starting compositions resembling Martian rocks under various temperature conditions (0–300 °C), CO_2 fugacities, and water-to-rock ratios (Bridges & Schwenzer, 2012; Bridges et al., 2015; Filiberto & Schwenzer, 2013; Griffith & Shock, 1995, 1997; Van Berk et al., 2011; Van Berk & Fu, 2011; Zolotov & Mironenko, 2016) but at predominantly low pressures and therefore relatively shallow depth. The secondary mineralogy in the nakhlites is best explained by percolating CO_2-rich hydrothermal fluids with initial temperatures between 150 and 200 °C, pH 6–8, and a water-to-rock ratio of ≤300 (Bridges & Schwenzer, 2012). Upon cooling of the fluids, Fe-rich phyllosilicate and subsequently an amorphous gel were precipitated (Bridges & Schwenzer, 2012; Changela & Bridges, 2011). The carbonate-bearing assemblages in nakhlites hence precipitated from rapidly cooling fluids and are likely metastable (Bridges et al., 2019). The zoned carbonate globules in the orthopyroxenite cumulate ALH 84001, however, likely formed at low temperatures presumably near 18 °C as suggested by carbon and oxygen isotope ratios (Halevy et al., 2011). A low temperature <150 °C is also suggested by experimental work (Golden et al., 2000, 2001) and geochemical modeling (Melwani Daswani et al., 2016; Van Berk et al., 2011) although formation conditions still remain relatively unconstrained. Furthermore, groundwater alteration processes at low temperature (~5 °C) and atmospheric CO_2 partial pressures between ~0.001 and 2 bars have been suggested by geochemical modeling as a possible formation mechanism for carbonate and phyllosilicate alteration in the Nili Fossae region (Van Berk & Fu, 2011). While the low temperatures match the observed Mg-rich carbonate above phyllosilicate stratigraphy on a smaller scale (Van Berk & Fu, 2011), the region was likely exposed to multiple alteration events under varying conditions due to extensive cratering including higher temperature fluids as suggested by the presence of prehnite (Ehlmann et al., 2011).

In particular, impact cratering and volcanism can induce large-scale, long-lasting hydrothermal systems on Mars resulting in the formation of the observed alteration minerals (Abramov & Kring, 2005; Costello et al., 2020; Crandall et al., 2021; Filiberto & Schwenzer, 2013; Griffith & Shock, 1995, 1997; Schwenzer & Kring, 2013). While most studies of hydrothermal alteration have focused on low-pressure environments and hence shallow depths, we are interested in low-grade metamorphic reactions at deeper levels and low fluid contents, resembling restricted fluid flow in the deeper subsurface. Here, we investigate the effect of variations in H_2O-CO_2 fluid compositions on a shergottite-like Martian basaltic and an ultramafic cumulate composition.

METHODS

Model Parameters

Phase diagrams are calculated with the Gibbs free energy minimization software Perple_X 6.8.9 (Connolly, 2005) using an internally consistent thermodynamic data set (Holland & Powell, 1998, 2002 update) following our previous approach (Semprich et al., 2019). MnO, Cr_2O_3, and P_2O_5 are excluded from the calculation because of their low abundance and/or limitation of solid solution models. Fe_2O_3 is defined by the following existing components: 2 FeO + 0.5 O_2 and is then set to 0 for reducing conditions and to a value corresponding to 10% of the total iron for more oxidizing conditions (resulting in ~1.5–2.5 wt% Fe_2O_3 for the compositions considered). All oxides are normalized to 100% by Perple_X. We use the following solid solution models (Table 1): clinopyroxene (Cpx), orthopyroxene (Opx), olivine (Ol), dolomite (Dol), and magnesite (Mgs) from Holland and Powell (1998); pumpellyite (Pmp), actinolite (Act), and stilpnomelane (Stp) from Massone and Willner (2008); chlorite (Chl) and white mica

Table 1. List of solid solutions and mineral formulae used in the models.

Mineral or solid solution, abbreviation used in Perple_X	Formulae of independent end members	Abbreviation	Reference
Pyroxenes			
Clinopyroxene, Cpx(HP)	*diopside:* $CaMgSi_2O_6$ *hedenbergite:* $CaFeSi_2O_6$ *jadeite:* $NaAlSi_2O_6$ *Ca-tschermaks:* $CaAl_2SiO_6$ *acmite:* $NaFe^{3+}Si_2O_6$	Cpx	Holland and Powell (1996, 1998)
Orthopyroxene, Opx(HP)	*enstatite:* $Mg_2Si_2O_6$ *ferrosilite:* $Fe_2Si_2O_6$ *Mg-tschermaks:* $MgAl_2SiO_6$ *Ferric tschermaks:* $MgFe^{3+}{}_2SiO_6$	Opx	Holland and Powell (1996, 1998)
Feldspars			
K-feldspar, Kf	*microcline:* $KAlSi_3O_8$ *albite:* $NaAlSi_3O_8$	Kfs	Thompson and Waldbaum (1969)
Plagioclase, Pl(h)	*high-albite:* $NaAlSi_3O_8$ *anorthite:* $CaAl_2Si_2O_8$	Pl	Newton et al. (1980)
Amphiboles			
Actinolite, Act(M)	*tremolite:* $Ca_2Mg_5Si_8O_{22}(OH)_2$ *actinolite:* $Ca_2Mg_3Fe_2Si_8O_{22}(OH)_2$ *glaucophane:* $Na_2Mg_3Al_2Si_8O_{22}(OH)_2$ *magnesioriebeckite:* $Na_2Mg_3Fe_2Si_8O_{22}(OH)_2$	Act	Massonne and Willner (2008)
Phyllosilicates			
Chlorite, Chl(W)	*clinochlore:* $Mg_5Al_2Si_3O_{10}(OH)_8$ *daphnite:* $Fe_5Al_2Si_3O_{10}(OH)_8$ *amesite:* $Mg_4Al_4Si_2O_{10}(OH)_8$ *Al-free-chlorite:* $Mg_6Si_4O_{10}(OH)_8$ *ferric chlinochlore:* $Mg_5Fe^{3+}AlSi_3O_{10}(OH)_8$	Chl	White et al. (2014)
Biotite, Bio(TCC)	*annite:* $KFe_3AlSi_3O_{10}(OH)_2$ *phlogopite:* $KMg_3AlSi_3O_{10}(OH)_2$ *eastonite:* $KMg_2Al_3Si_2O_{10}(OH)_2$ *ferric biotite:* $KMg_2Fe^{3+}Al_2Si_2O_{10}(OH)_2$	Bt	Tajčmanová et al. (2009)

Table 1. *Continued*. List of solid solutions and mineral formulae used in the models.

Mineral or solid solution, abbreviation used in Perple_X	Formulae of independent end members	Abbreviation	Reference
White mica, Mica (W)	*muscovite:* $KAl_3Si_3O_{10}(OH)_2$ *paragonite:* $NaAl_3Si_3O_{10}(OH)_2$ *margarite:* $CaAl_4Si_2O_{10}(OH)_2$ *celadonite:* $KMgAlSi_4O_{10}(OH)_2$ *ferrous celadonite:* $KFeAlSi_4O_{10}(OH)_2$ *ferric muscovite:* $KFe^{3+}Al_2Si_3O_{10}(OH)_2$	Ms	White et al. (2014)
Stilpnomelane, Stp(M)	*stilpnomelane:* $K_5Al_5Fe_{48}Si_{67}O_{168}(OH)_{48}\cdot 36H_2O$ *magnesio-stilpnomelane:* $K_5Al_5Mg_{48}Si_{67}O_{168}(OH)_{48}\cdot 36H_2O$	Stp	Massonne and Willner (2008)
Serpentine, Atg(PN)	*antigorite:* $Mg_{48}Si_{34}O_{85}(OH)_{62}$ *Fe-antigorite:* $Fe_{48}Si_{34}O_{85}(OH)_{62}$	Atg	Padrón-Navarta et al. (2013)
Talc, T	*talc:* $Mg_3Si_4O_{10}(OH)_2$ *Fe-talc:* $Fe_3Si_4O_{10}(OH)_2$ *talc-tschermaks:* $Mg_2Al_2Si_3O_{10}(OH)_2$	Tlc	Ideal
Zeolites			
Laumontite	$CaAl_2Si_4O_{12}\cdot 4H_2O$	Lmt	Pure
Stilbite	$CaAl_2Si_7O_{18}\cdot 7H_2O$	Stb	Pure
Wairakite	$CaAl_2Si_4O_{12}\cdot 2H_2O$	Wrk	Pure
Other silicates			
Prehnite	$Ca_2Al_2Si_3O_{10}(OH)_2$		Pure
Pumpellyite, Pu(M)	*pumpellyite:* $Ca_4MgAl_5Si_6O_{21}(OH)_7$ *ferro-pumpellyite:* $Ca_4FeAl_5Si_6O_{21}(OH)_7$ *ferri-pumpellyite:* $Ca_4MgFe_5Si_6O_{21}(OH)_7$	Pmp	Massonne and Willner (2008)
Epidote, Ep (HP11)	*Fe-epidote:* $Ca_2Fe_2AlSi_3O_{12}(OH)$ *clinozoisite:* $Ca_2Al_3Si_3O_{12}(OH)$	Ep	Holland and Powell (2011)
Olivine, O(HP)	*forsterite:* Mg_2SiO_4 *fayalite:* Fe_2SiO_4	Ol	Holland and Powell (1998)
Titanite (sphene)	$CaTiSiO_5$	Ttn	Pure
Quartz	SiO_2	Qz	Pure
Lawsonite	$CaAl_2Si_2O_7(OH)_2\cdot H_2O$	Lws	Pure
Carbonates			
Calcite	$CaCO_3$	Cal	Pure
Dolomite, Do(HP)	*dolomite:* $CaMg(CO_3)_2$ *ankerite:* $CaFe(CO_3)_2$		Holland and Powell (1998)

Table 1. *Continued*. List of solid solutions and mineral formulae used in the models.

Mineral or solid solution, abbreviation used in Perple_X	Formulae of independent end members	Abbreviation	Reference
Magnesite, M(HP)	*magnesite:* $MgCO_3$ *siderite:* $FeCO_3$		Holland and Powell (1998)
Oxides/Hydroxides			
Ilmenite, Ilm(WPH)	*ilmenite:* $FeTiO_3$ *geikielite:* $MgTiO_3$ *hematite:* $Fe^{3+}{}_2O_3$	Ilm	White et al. (2000)
Spinel, Sp(HP)	*spinel:* $MgAl_2O_4$ *hercynite:* $FeAl_2O_4$	Sp	Holland and Powell (1998)
Magnetite	Fe_3O_4	Mag	Pure
Brucite, B	*brucite:* $Mg(OH)_2$ *Fe-brucite:* $Fe(OH)_2$	Brc	Ideal

(abbreviated as Ms) from White et. al. (2014); epidote (Ep) from Holland and Powell (2011); biotite from Tajčmanová et al. (2009); antigorite (Atg) from Padrón-Navarta et al. (2013); K-feldspar (Kfs) from Thompson and Waldbaum (1969); plagioclase (Pl) from Newton et al. (1980); ilmenite (Ilm) from White et al. (2000). Talc (Tlc) and brucite (Brc) were assumed to be ideal solutions. Quartz (qz), prehnite (prh), calcite (cal, and aragonite in the low-temperature, high-pressure section of the diagrams), stilbite (stlb), laumontite (lmt), wairakite (wrk), lawsonite (lws), rutile (rt), titanite (ttn), and magnetite (mag) are treated as pure phases. Vesuvianite and garnet (andradite) are excluded since their modeled stabilities exceed those in real rocks and they have not been detected on Mars. Fluid (F) is represented by a C-O-H generic hybrid equation-of-state fluid model (Connolly, 1995) allowing for the following species: H_2O, CO_2, CH_4, H_2, CO. The internal molecular fluid equation of state for pure H_2O and CO_2 species is set to a Compensated-Redlich–Kwong equation, which allows the calculation of the volumes and fugacities of H_2O and CO_2 over a large pressure and temperature range (Holland & Powell, 1991, 1998).

Input Parameters

Protolith Compositions

We use the starting compositions of Bounce Rock (Zipfel et al., 2011) and a poikilitic shergottite ALHA77005 (Lodders, 1998) as representative Martian mafic and ultramafic rocks, respectively (Table 2). Bounce Rock resembles basaltic shergottite meteorites in texture, mineralogy, and chemistry, in particular lithology B of EETA79001 and QUE 94201 (Zipfel et al., 2011). For both compositions, we assume two different oxidation states (1) all iron is assumed to be divalent FeO; and (2) 10% of the iron is assumed to be trivalent Fe_2O_3, and the remainder divalent, which gives 1.55 wt% Fe_2O_3 and 2.23 wt% Fe_2O_3 for Bounce Rock and ALHA77005, respectively. The chosen range covers the redox states measured for the majority of Martian basalts (e.g., Herd, 2003; Schmidt et al., 2013).

Fluid Content and Composition

While the fluid content of the deeper Martian subsurface now and at earlier time periods is not known, the present-day estimates by gamma ray spectroscopy of surface rocks range between 1.5% and 7.5 wt% H_2O in low- and mid-latitude regions (Boynton et al., 2007). A similar near-surface water range of 2–7 wt% (Wernicke & Jakosky, 2021) was estimated based on data obtained by the Mars Odyssey Neutron Spectrometer (MONS; Feldman et al., 2004; Maurice et al., 2011) and the 3 μm absorption of the Observatoire pour la Minéralogie, l'Eau, les Glaces et l'Activité (OMEGA; Audouard et al., 2014; Milliken et al., 2007). Furthermore, Curiosity's Dynamic Albedo of Neutron (DAN) instrument yields estimates between 1.5 and 3.3 wt% and up to ~5 wt% water locally within the upper 60 cm below the surface (Litvak et al., 2016;

Table 2. Starting bulk compositions for basaltic (Bounce Rock; Zipfel et al., 2011) and ultramafic (ALHA77005; Lodders, 1998) Martian protoliths with only FeO (red) and 10% Fe_2O_3 (ox).

Oxides (wt%)	Bounce Rock (red)	Bounce Rock (ox)	ALHA77005 (red)	ALHA77005 (ox)
SiO_2	51.6	51.6	42.2	42.2
TiO_2	0.74	0.74	0.39	0.39
Al_2O_3	10.5	10.5	2.9	2.9
FeO	14.4	13.0	20.1	18.0
Fe_2O_3	0	1.55	0	2.23
MgO	6.8	6.8	28.2	28.2
CaO	12.1	12.1	3.2	3.2
Na_2O	1.7	1.7	0.47	0.47
K_2O	0.1	0.1	-	-

Mitrofanov et al., 2014). Measurements of bedrock in the Murray formation by ChemCam laser-induced breakdown spectroscopy estimate a similar range of 2.3–3.1 wt% H_2O (Thomas et al., 2020). The percentages for the Martian soil at Gale crater are likely derived from both adsorbed water molecules in the regolith and water structurally bound in minerals (Mitrofanov et al., 2014). While the H_2O content of adsorbed water in the deeper crust is unknown, phyllosilicates have been excavated by impact cratering from depths of at least 7 km and even up to 17 km for one impact event (Flahaut et al., 2012; Mustard, 2019; Mustard et al., 2008; Sun & Milliken, 2015). This would suggest that at least the upper 10 km of the crust contains structurally bound water in the form of hydrous minerals (Mustard, 2019). Estimates of average subsurface water content range between 0.5 and 3 wt% (Mustard, 2019; Wernicke & Jakosky, 2021) although regional differences may result in locally higher values. Modeling of low-grade metamorphic phases as a function of water availability has shown that ~2.5 wt% H_2O is required for the formation of prehnite in basaltic rocks and ~2.7 wt% for serpentine in ultramafic compositions, while the zeolites laumontite and analcime require ~4 wt% and 5.2 wt% H_2O, respectively (Semprich et al., 2019). To include these important low-grade metamorphic phases in our models, we have therefore chosen to compute phase equilibria at somewhat higher fluid content than the estimated average for the Martian subsurface.

The amount of CO_2 in the subsurface is not well constrained. The Martian dust contains 2–5 wt% carbonates according to detections by remote sensing from orbit (Bandfield et al., 2003), and soils contain up to 1 wt% (Archer et al., 2014). However, in situ measurements by the Spirit rover in Gusev crater identified carbonates within localized outcrops in abundances of 16–34 wt% (Morris et al., 2010). Based on their relative limited detection, Hu et al. (2015) estimate the amount of carbonates in the crust to range between 1 and 5 wt%. Similar to estimates of the water content, regional variations are likely as shown by the low amounts of carbonates in large parts of Gale crater until the recent detection of siderite (Archer et al., 2020).

Based on measured values and mineralogical restrictions, we use two setups for our calculations including (1) a model where the amount of fluid in the system is restricted to 5 wt% and its composition is varied from H_2O-dominated to CO_2-dominated and (2) a fluid-saturated model with the fluid composition defined by $X(CO_2)$. In calculations with a saturated fluid, O_2 is set as an unconstrained saturated component to be consistent with C-O-H fluid speciation instead of specifying FeO/Fe_2O_3 in the starting composition. In this setup, we exclude all COH fluid species other than H_2O, CO_2, and O_2.

Further Model Parameters

Until the availability of in situ measurements, estimates of the surface heat flux of Mars and resulting geothermal gradients are based on indirect methods relying on several poorly constrained parameters such as the abundance of heat-producing elements, topography, crust and mantle thickness and their densities (e.g., McGovern et al., 2002, 2004; Parro et al., 2017; Plesa et al., 2016). The estimated heat flow in Noachian terrains ranges from >35 to 60 mW m^{-2} corresponding to thermal gradients between >14 and 20 °C km^{-1} (McGovern et al., 2004) and a Noachian geotherm of 12 °C km^{-1} has been calculated for the Nili Fossae region (McSween et al., 2015), which shows an abundance of low-grade minerals and carbonate detections (e.g., Ehlmann, Mustard, Murchie, et al., 2008; Ehlmann et al., 2011). Based on these values, we selected 10, 13, and 20 °C km^{-1} geotherms in all calculated phase diagrams. Mineral modes as a function of fluid composition are only extracted along the 13 and 20 °C km^{-1} geotherms since assemblages formed along these gradients are more likely to contain the characteristic low-grade metamorphic minerals such as prehnite and zeolites.

For depth estimates from pressure, we use the following equation: $h = P/\rho g$, where the gravity (g) for Mars is assumed to be 3.727 m s^{-2} and the average crustal density (ρ) is 2900 kg m^{-3}, a commonly used value in Mars models (e.g., McGovern et al., 2004; Parro et al., 2017; Plesa et al., 2016; Sohl et al., 2005). However, any depth estimates given in this work should be taken as a rough approximation since the actual density is not constant and varies with the extent of

Fig. 1. Phase stability fields for the composition of Bounce Rock with fluid limited to 5 wt% in the range of 150–450 °C and 0–0.5 GPa using starting compositions with FeO only (a, c, e), and 1.55 wt% Fe_2O_3, equivalent to 10% of FeO_{tot} (b, d, f). The CO_2 content in the bulk composition is increased from top to bottom with 0 wt% CO_2 (a, b); 1 wt% CO_2 (c, d), and 2 wt% CO_2 (e, f). Mineral abbreviations (solid solutions capitalized; pure phases lowercase): Act = actinolite; Bt = biotite; cal = calcite; Chl = chlorite, Cpx = clinopyroxene; Dol = dolomite; Ep = epidote; F = COH-Fluid, ilm = ilmenite, Kfs = K-feldspar, lmt = laumontite, lws = lawsonite, Ms = muscovite (white mica), Pl = plagioclase, Pmp = pumpellyite, prh = prehnite, qz = quartz, stlb = stilbite, Stp = stilpnomelane, ttn = titanite, wrk = wairakite. Small fields are not labeled. Colored areas indicate the stability fields of characteristic low-grade minerals relevant for Mars: red = pumpellyite, yellow = prehnite, blue = epidote, orange = pumpellyite + prehnite, green = epidote + prehnite, purple = pumpellyite + prehnite, turquoise = pumpellyite + epidote + prehnite. Textures indicate stabilities of several zeolites. Minerals in bold have been reported as alteration phases in the Nili Fossae area (e.g., McSween et al., 2015), in particular the assemblage prehnite + chlorite, unspecified zeolites (which are represented here as stilbite, laumontite, and wairakite), albite, shown here as Kfs, and Fe/Mg carbonates (here as dolomite). Potential mineral detections are in bold italic including quartz (which is detected as opaline silica), epidote, and muscovite. Solid black lines represent geotherms at 10, 13, and 20 °C km^{-1}, respectively. Red circles on the geotherms represent conditions at which mineral modes are extracted for Fig. 2.

fracturing and of compaction from overburden pressure in the upper crust (Clifford, 1993) and as a function of pressure at depth (e.g., Semprich & Filiberto, 2020).

RESULTS

Mineral Stabilities in Basaltic Compositions with Variation in H_2O-CO_2

Mineralogy of Bounce Rock with 5 wt% Bulk Fluids

Figure 1 shows phase stability diagrams calculated for the composition of Bounce Rock (Table 2) with only divalent iron (Figs. 1a, 1c, and 1e), and 1.55 wt% Fe_2O_3 representing 10% of FeO_{tot} recalculated to be trivalent (Figs. 1b, 1d, and 1f). The amount of fluid in the bulk composition is set to 5 wt% and increases in CO_2 from top to bottom with 0 wt% CO_2 (Figs. 1a and 1b), 1 wt% CO_2 (Figs. 1c and 1d), and 2 wt% CO_2 (Figs. 1e and 1f). Figure 2 shows mineral modes as a function of CO_2 (mol kg^{-1}) in the bulk composition at 200 °C on the 13 and 20 °C km^{-1} geotherms (indicated by red circles in Fig. 1).

The prehnite stability field (shown in yellow in Fig. 1) is largest in calculations with divalent iron and pure H_2O fluids in the temperature range of 150 °C to ~320 °C and pressures ≤0.37 GPa (Fig. 1a). In the modeled composition with trivalent iron, prehnite stability is reduced toward lower pressures (≤0.3 GPa) due to the presence of pumpellyite and toward lower temperatures (≤280 °C) due to the presence of epidote. Prehnite is stable together with pumpellyite (orange field, Fig. 1) and epidote (green field; Fig. 1). In compositions with as little as 1 wt% CO_2, prehnite stability is decreased significantly for both reduced and oxidized conditions (Figs. 1c and 1d); however, its stability is still larger in the composition with divalent iron (Fig. 1c). In the composition with trivalent iron, prehnite occurs predominantly with epidote, pumpellyite, or both (Fig. 1d). Compositions with >2 wt% CO_2 have no prehnite (Figs. 1e and 1f). Prehnite is present in up to ~20 vol% in the composition with no Fe_2O_3 at 200 °C on both the 20 and 13 °C km^{-1} geotherms (Figs. 2a and 2c) and at lower CO_2, but is not stable above ~0.44 mol kg^{-1} (1.9 wt%) CO_2. In compositions with 1.55 wt% Fe_2O_3, prehnite is only present at 200 °C on the 20 °C km^{-1} geotherm up to 15 vol% and coexists with pumpellyite at low CO_2 of ≤0.26 mol kg^{-1} (1.13 wt %) and is not stable >0.44 mol kg^{-1} CO_2. At 200 °C on the 13 °C km^{-1} geotherm, prehnite is not stable. Hence, our models predict prehnite formation in less oxidized, CO_2-poor environments and predominantly along warmer geotherms.

Pumpellyite is stable in modeled compositions with divalent and trivalent iron and pure H_2O and limited CO_2 fluids but absent at higher CO_2 of 2 wt% (Figs. 1a–d). In calculations with divalent iron, pumpellyite replaces prehnite above ~0.1 GPa at 150 °C and at higher pressures with increasing temperature (Figs. 1a and 1c). In compositions with trivalent iron, pumpellyite is stable with prehnite at lower pressures (Figs. 1b and 1d). In calculations with 1 wt% CO_2, pumpellyite stability is extended toward higher pressures, since calcite replaces the Ca-bearing lawsonite (Figs. 1c and 1d). Pumpellyite is not stable in compositions with divalent iron at 200 °C on the 13 and 20 °C km^{-1} geotherms (Figs. 2a and 2c). In calculations with trivalent iron on the 20 °C km^{-1} geotherm (Fig. 2b), pumpellyite is stable in up to 15 vol% together with prehnite at low CO_2 of ≤0.26 mol kg^{-1} (1.13 wt%). Pumpellyite is present in amounts of >20 vol% in models with trivalent iron on the 13 °C km^{-1} geotherm, where prehnite is absent (Fig. 2d). According to our models, pumpellyite would be expected in CO_2-poor conditions at higher pressures and hence on colder geotherms and is more stable in compositions with trivalent iron.

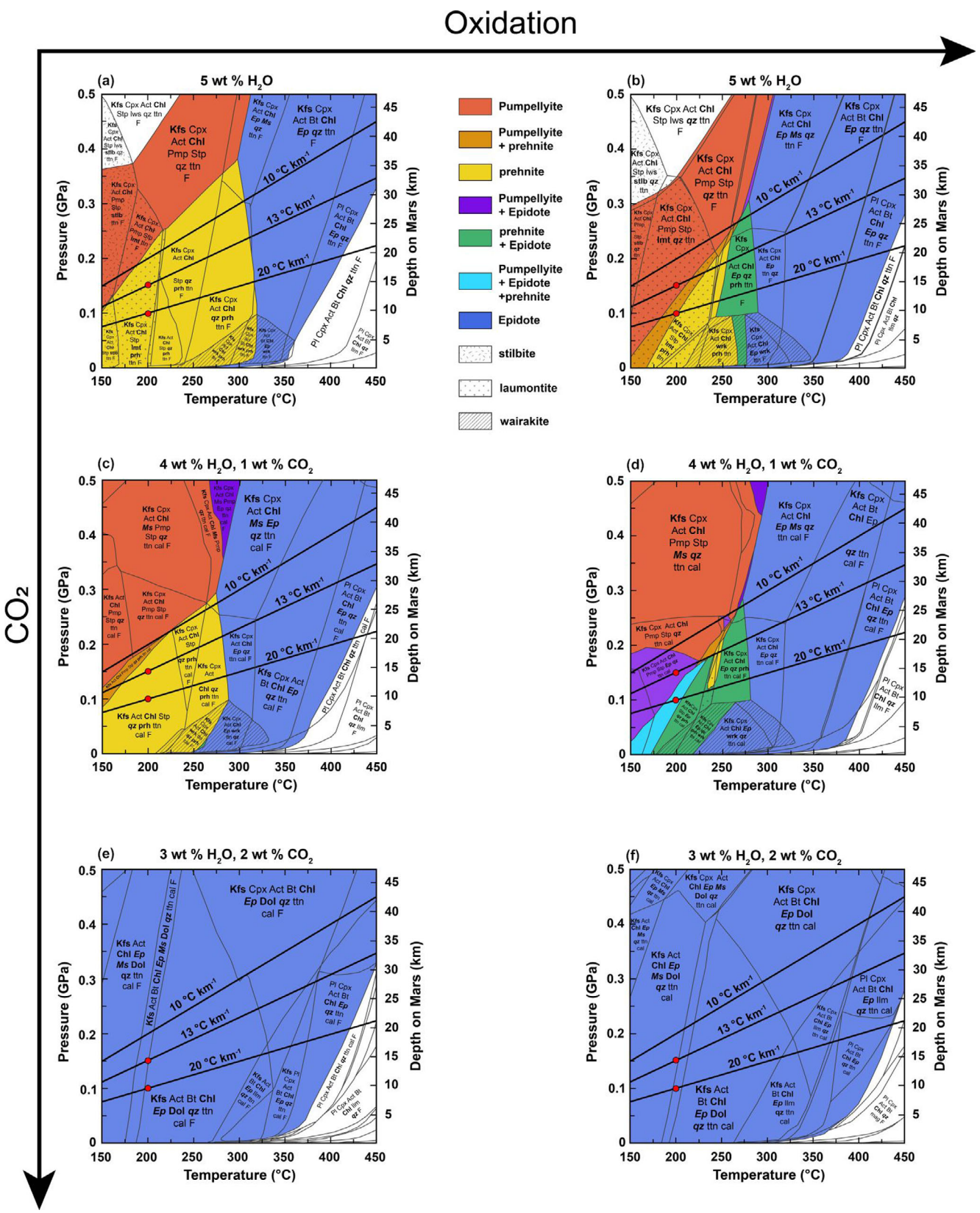
Oxidation
CO2
(a) 5 wt % H2O
(b) 5 wt % H2O
(c) 4 wt % H2O, 1 wt % CO2
(d) 4 wt % H2O, 1 wt % CO2
(e) 3 wt % H2O, 2 wt % CO2
(f) 3 wt % H2O, 2 wt % CO2
Pressure (GPa)
Depth on Mars (km)
Temperature (°C)
10 °C km-1
13 °C km-1
20 °C km-1
Pumpellyite
Pumpellyite + prehnite
prehnite
Pumpellyite + Epidote
prehnite + Epidote
Pumpellyite + Epidote +prehnite
Epidote
stilbite
laumontite
wairakite

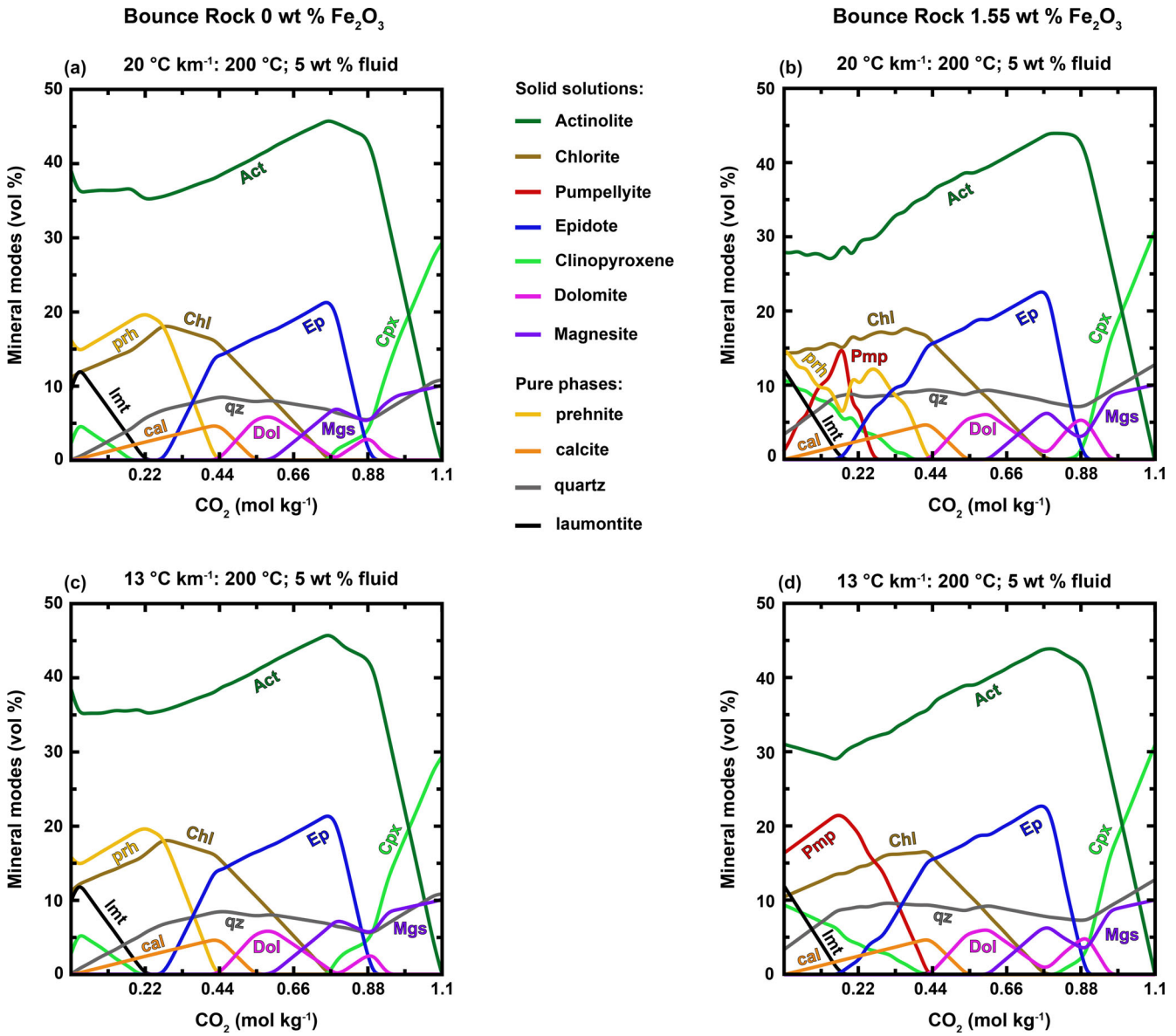

Fig. 2. Modes (vol%) for selected minerals in the basaltic starting composition of Bounce Rock with 5 wt% of fluid varying from 0 to 5 wt% CO_2 plotted as a function of CO_2 (mol kg^{-1}) in the bulk composition at 200 °C on geotherms of 20 °C km^{-1} (a, b), and 13 °C km^{-1} (c, d) assuming only divalent iron (a, c) and 1.55 wt% Fe_2O_3 (b, d). See Fig. 1 for mineral abbreviations (solid solutions capitalized, pure phases lowercase).

Epidote is stable at temperatures >250 °C in modeled compositions with divalent iron and with 0–1 wt% CO_2 (Figs. 1a and 1c). Epidote stability is shifted toward lower temperatures (150 °C) in calculations with trivalent iron at 1 wt% CO_2 (Fig. 1d). In compositions with 2 wt% CO_2, epidote replaces prehnite, pumpellyite, and zeolites at all temperatures considered (Figs. 1e and 1f). Epidote is stable in the range of 0.28–0.88 mol kg^{-1} CO_2 (1.2–3.9 wt%) up to 22 vol% in compositions with divalent iron on both geotherms (Figs. 2a and 2c). In calculations with trivalent iron, epidote stability is shifted toward lower CO_2 levels of 0.17 mol kg^{-1} (0.76 wt%) on both geotherms (Figs. 2b and 2d). Therefore, epidote in our models is stable at higher CO_2 levels and coexists with dolomite and magnesite in contrast to other Ca-Al-bearing phases such as pumpellyite, prehnite, and zeolites.

The zeolites stilbite, laumontite, and wairakite are stable in the compositions with no CO_2 (Figs. 1a and 1b). Their stability is reduced significantly in compositions with only 1 wt% CO_2, where stilbite is

absent at all oxidation states. Laumontite is absent in the composition with divalent iron and present in a limited P–T range in the composition with trivalent iron, while wairakite is still present in both compositions (Figs. 1c and 1d). At 2 wt% CO_2 (Figs. 1e and 1f), zeolites are absent. Both the 20 and 13 °C km^{-1} geotherms predominantly pass through the laumontite stability field, which is therefore the only stable zeolite occurring in ~≤12 vol% at conditions considered in Fig. 2. Laumontite decreases rapidly with an increase in CO_2 and is not stable above 0.22 mol kg^{-1} (~0.97 wt%) CO_2.

Calcite forms as soon as CO_2 is added to the fluid composition and occurs in <5 vol% together with laumontite, prehnite, and pumpellyite. At ~0.44 mol kg^{-1} CO_2, dolomite replaces calcite at <6 vol %. Magnesite forms at ~0.6 mol kg^{-1} (~2.7 wt%) CO_2 and increases in abundance to ~10 vol% with CO_2-dominant fluids.

Actinolite is a ubiquitous phase (≤45 vol%) in all modeled conditions and is only absent where the fluid is pure CO_2 (Fig. 2). Chlorite is present at lower CO_2 in ≤18 vol% and is not stable above ~0.77 mol kg^{-1} (3.42 wt% CO_2) on both geotherms and oxidation states (Fig. 2). Micas are present in low amounts <5 vol % at the conditions considered (not shown in Fig. 2 but listed in Table S1 in supporting information). Stilpnomelane is present at low temperatures and low CO_2. Biotite is present at higher temperatures and CO_2 but in low amounts of <1 vol%. White mica (muscovite) is stable at higher pressures and would be expected on colder geotherms of 10 °C km^{-1} (Fig. 1). Lawsonite is present in the phase diagrams at high pressures, low temperatures, and low CO_2 (Figs. 1a and 1b) but is not expected to occur on Martian geotherms.

Feldspars are present at all modeled pressure–temperature conditions with the K-feldspar solid solution (of predominantly albite composition) stable at lower temperatures and plagioclase at higher temperatures and higher CO_2 (Table S1). K-feldspar abundance is not significantly influenced by an increase in CO_2 in the fluid composition and is present up to ~17 vol% (not shown in Fig. 2). Plagioclase is stable above ~0.8 mol kg^{-1} (3.5 wt%) CO_2 on both geotherms and increases with an increase in CO_2 up to 24 vol%.

Quartz is present in relatively small amounts of ~4 vol% at H_2O-rich conditions but increases with an increase in CO_2 to ~11 vol% (Fig. 2). Clinopyroxene is stable at low CO_2 and again at high CO_2 with up to 30 vol% (Fig. 2). Orthopyroxene forms at high CO_2 of ~0.98 mol kg^{-1} (4.3 wt%) in ≤9 vol% (not shown in Fig. 2). Titanite, ilmenite, magnetite, and a fluid phase are present as accessory phases in ≤2 vol% (see Table S1).

Mineralogy of Bounce Rock with a Saturated Fluid

Figure 3 shows mineral modes in Bounce Rock at 200 °C on the 20 and 13 °C km^{-1} geotherms as a function of $X(CO_2)$ at fluid-saturated conditions assuming the fluid phase components H_2O and CO_2 are always present in sufficient quantity to saturate the system. In calculations for the 20 °C km^{-1} geotherm (Fig. 3a), epidote and clinopyroxene are only stable at very low $X(CO_2)$. Laumontite is stable up to $X(CO_2)$ ~0.00063 (~4.7 wt% H_2O and 6.7 wt% CO_2 or 1.5 mol kg^{-1} in the bulk composition). Above this value, the assemblage is dominated by quartz (~35 vol %), calcite (~21 vol%), chlorite (~18 vol%), and muscovite (~14 vol%). K-feldspar is also present in ~4 vol%. Additional phases include ilmenite and rutile (not shown in Fig. 3). On the 13 °C km^{-1} geotherm (Fig. 3b), laumontite is stable to $X(CO_2)$ ~0.00028 and the assemblage at high $X(CO_2)$ is dominated by quartz, calcite, chlorite, and muscovite.

Mineral Stabilities in Ultramafic Compositions with Variation in H_2O-CO_2

Mineralogy of the Ultramafic Composition with 5 wt% Bulk Fluids

Figure 4 shows mineral modes as a function of bulk CO_2 (mol kg^{-1}) for the ultramafic composition of ALH 77005 (Table 2) at 200 °C on the 20 °C km^{-1} (Figs. 4a and 4b) and 13 °C km^{-1} geotherms (Figs. 4c and 4d) with only divalent iron (Figs. 4a and 4c) and 2.23 wt% Fe_2O_3 (Figs. 4b and 4d). Antigorite (serpentine) is a dominant phase (≤36 vol%) for all modeled conditions at low CO_2 and is not stable above ~0.26 mol kg^{-1} (1.2 wt%) CO_2 on the 20 °C km^{-1} geotherm and ~0.33 mol kg^{-1} (1.4 wt%) CO_2 on the 13 °C km^{-1} geotherm. Talc is stable in the range between ~0.05 mol kg^{-1} (0.2 wt%) and ~0.62 mol kg^{-1} (2.7 wt %) CO_2 on the 20 °C km^{-1} geotherm and between ~0.09 mol kg^{-1} (0.4 wt%) and 0.96 mol kg^{-1} (4.2 wt%) CO_2 on the 13 °C km^{-1} geotherm. Magnesite is the first and only carbonate forming in all compositions at ~0.14 mol kg^{-1} (~0.6 wt%) CO_2, increasing in abundance with CO_2 up to ~11 vol% on the 20 °C km^{-1} geotherm, and at ~0.34 mol kg^{-1} (1.5 wt %) CO_2 on the 13 °C km^{-1} at ≤9 vol% in a pure CO_2 fluid. Actinolite (≤32 vol%) is present at most conditions except at pure CO_2. Chlorite abundance increases up to ~18 vol% at lower CO_2 but decreases at higher CO_2 and is not stable above ~0.96 mol kg^{-1} (4.2 wt%) CO_2 on the 20 °C km^{-1} geotherm and ~0.72 mol kg^{-1} (3.2 wt%) CO_2 on the 13 °C km^{-1} geotherm. Olivine is a stable phase at all conditions but is less abundant where talc is present. Clinopyroxene is present at CO_2-poor and CO_2-rich conditions.

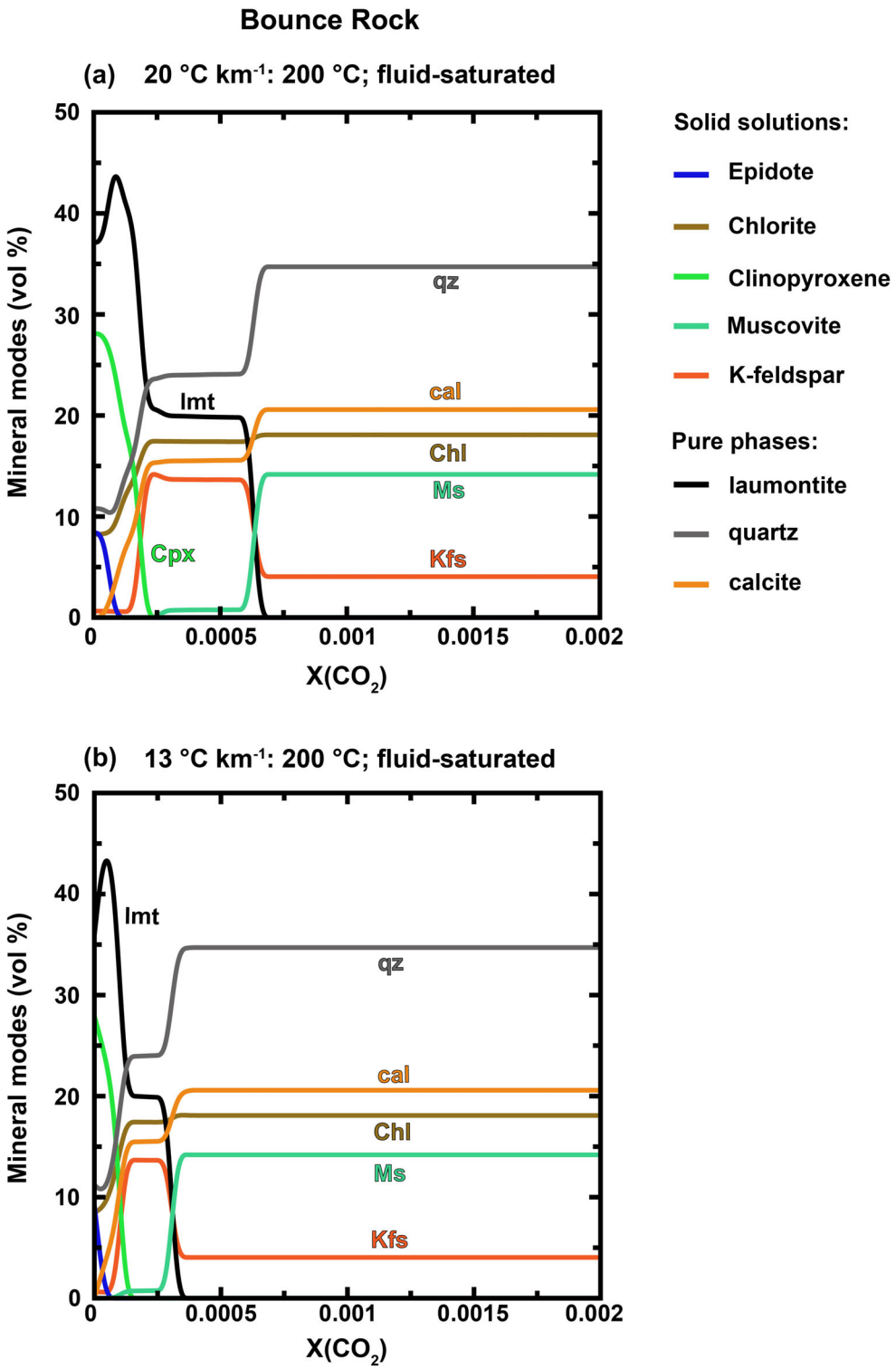

Fig. 3. Modes (vol%) for selected minerals in the basaltic starting composition of Bounce Rock assuming fluid- and O_2-saturated conditions at 200 °C on the 20 °C km^{-1} (a), and 13 °C km^{-1} (b) geotherms. See Fig. 1 for mineral abbreviations (solid solutions capitalized, pure phases lowercase).

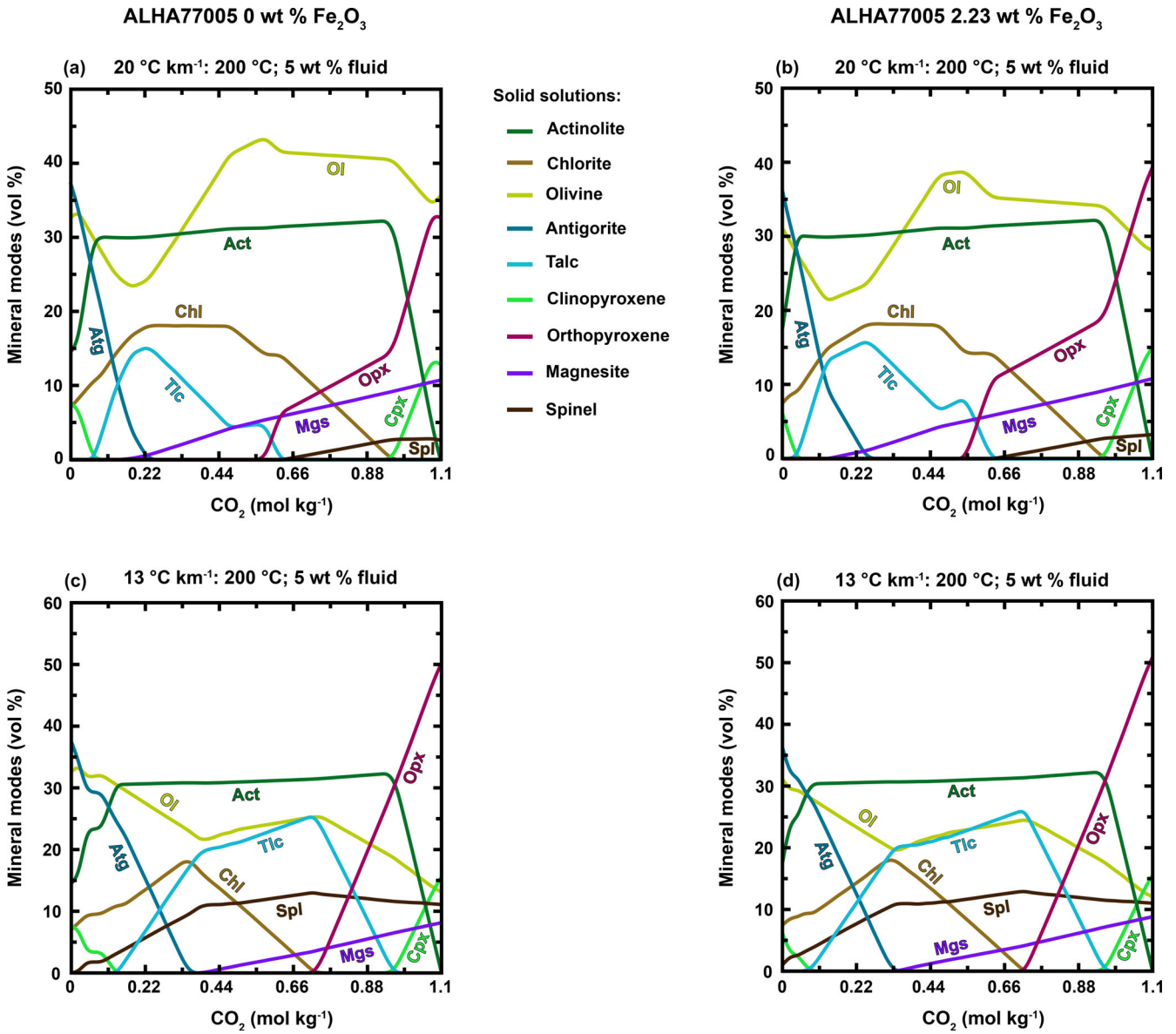

Fig. 4. Modes (vol%) for selected minerals in the ultramafic starting composition of ALHA77005 with 5 wt% of fluid varying from 0 to 5 wt% CO_2 plotted as a function of CO_2 (mol kg^{-1}) in the bulk composition at 200 °C on geotherms of 20 °C km^{-1} (a, b), and 13 °C km^{-1} (c, d) assuming only divalent iron (a, c) and 2. 23 wt% Fe_2O_3 (b, d). Act = actinolite; Atg = antigorite; Chl = chlorite; Cpx = clinopyroxene; Mgs = magnesite; Ol = olivine; Opx = orthopyroxene; Spl = spinel; Tlc = talc.

Orthopyroxene forms at ~0.57 mol kg^{-1} (2.5 wt%) CO_2 on the 20 °C km^{-1} geotherm and reaches ~39 vol% at maximum CO_2. On the 13 °C km^{-1} geotherm, orthopyroxene forms at ≥0.73 mol kg^{-1} (3.2 wt%) CO_2 at ~50 vol% at maximum CO_2. Spinel forms at higher CO_2 on the 20 °C km^{-1} geotherm and is present at all conditions on the 13 °C km^{-1} geotherm. Ilmenite and magnetite (not shown in Fig. 4) are also stable at most conditions. K-feldspar (not shown) only forms in CO_2-rich conditions.

Mineralogy of the Ultramafic Composition with a Saturated Fluid

Figure 5 shows mineral modes of the ALH77005 composition at 200 °C on the 20 and 13 °C km^{-1} geotherms as a function of $X(CO_2)$ at fluid-saturated conditions. On the 20 °C km^{-1} geotherm, calcite forms at low $X(CO_2)$ but is replaced by dolomite at $X(CO_2)$. Antigorite is not stable above ~0.0035 $X(CO_2)$ or ~1.06 mol kg^{-1} (4.6 wt%) CO_2 in the bulk composition, and the assemblage is dominated by talc (~53 vol%),

chlorite (~17 vol%), and dolomite (~10 vol%) with lesser amounts of actinolite (~6 vol%) and magnesite (~4 vol%).

On the 13 °C km^{-1} geotherm (Fig. 5b), calcite is the first carbonate to form in small quantities at low X (CO_2) but is replaced by dolomite at 0.0006 X(CO_2), equivalent to 1.05 mol kg^{-1} (4.6 wt%) CO_2 in the bulk composition. Magnesite forms at ~0.0019 X(CO_2). Antigorite is not stable above ~0.0018 X(CO_2). At higher X(CO_2), the assemblage is dominated by talc (~53 vol%) and chlorite (~17 vol%), with lesser amounts of dolomite (~10 vol%), actinolite (~6 vol%), and magnesite (~4 vol %). Talc is stable up to ~0.0035 X(CO_2) or 1.55 mol kg^{-1} (6.8 wt%) CO_2 in the bulk composition. At X(CO_2) >0.0035, the assemblage is dominated by magnesite (~32 vol%) and quartz (~31 vol%) with lesser amounts of chlorite (~14 vol%), dolomite (~9 vol%), and actinolite (~5 vol%). Ilmenite is present at all conditions (~10 vol%) while small quantities of titanite occur at low X(CO_2) and rutile at higher X(CO_2).

DISCUSSION

Limitations of the Model

Our calculations assume thermodynamic equilibrium, which may not be achieved everywhere at low-temperature conditions with slow reaction rates on Mars. For instance, the carbonate assemblages in nakhlite meteorites are likely metastable (e.g., Bridges et al., 2019). However, we consider these phase equilibria calculations as good approximations to model subsurface low-grade metamorphic processes on Mars, since we assume a relatively closed system at depth where fluids are present in the pore space and can, therefore, react with the rocks over geological time scales. It is very likely that Martian basaltic rocks preserve their textures at low-grade metamorphic conditions as observed in terrestrial metabasic volcanic rocks, where alteration phases form in veins and vesicles that are more accessible to fluids (e.g., Cho & Liou, 1987; Starkey & Frost, 1990). Nevertheless, it can be assumed that at least locally the fluid is equilibrated with the rock to form characteristic alteration phases, but these textural relationships may explain why our models predict abundant actinolite, while it is not observed in most spectral studies (see Semprich et al., 2019, for a detailed discussion of this issue).

Our models specifically address the influence of CO_2 on mineral stabilities, and we therefore did not consider Cl, F, or S in our calculations. High-temperature Martian fluids are enriched in Cl as indicated by Cl-bearing phases in meteorites (e.g., Filiberto et al., 2014; Viennet et al., 2020), and low-grade metamorphic assemblages may therefore also be influenced by these elements. However, thermodynamic data for minerals including halogens are scarce and therefore currently not available in the thermodynamic database for the phases of importance for low-grade metamorphic conditions. Subsurface fluids on Mars may also likely increase in salinity if they are comparable to deep waters on Earth (Möller et al., 1997; Nurmi et al., 1988), which is not considered in our calculations. We also do not consider the oxides MnO, P_2O_5, and Cr_2O_3 in the starting composition, which are relatively low and are therefore not expected to significantly influence the calculated mineral assemblages although they could cause minor changes in phase stability fields and mineral abundances.

Effect of Oxidation State on Mineral Stability

In addition to the protolith composition, the oxygen fugacity during metamorphism is also influenced by the fluid, adding further uncertainties. A large range of oxygen fugacities has been reported for Martian igneous rocks (e.g., Herd, 2006; Schmidt et al., 2013). Therefore, we cover most of the range of possible Martian oxygen fugacities by assuming two endmember compositions with only divalent iron and 10% of the total iron as trivalent iron. Uncertainties may arise due to limited thermodynamic data on Fe^{3+} members or the lack of solid solution models including Fe^{3+} endmembers, which is discussed for prehnite below.

In Bounce Rock, changes in oxidation state mainly affect the stability of prehnite, pumpellyite, and epidote with a decrease in the prehnite stability field toward lower pressures and temperatures in the compositions including trivalent iron (Figs. 1 and 2). While pumpellyite and epidote can be modeled with solid solutions including Fe^{3+} endmembers, prehnite is assumed to be a pure phase and therefore does not allow for Fe^{3+} substitution in our calculations. As a result, the stability fields of pumpellyite and epidote are increased at more oxidizing conditions. However, in natural prehnite, Fe^{3+} can replace octahedral Al according to $Ca_2Al_{1-x}Fe_x(AlSi_3O_{10})(OH)_2$, where x denotes the amount of moles of substitution. Fe^{3+}-rich prehnite occurs in hydrothermal settings with mole fractions of Fe^{3+} as high as ~0.6 (Freedman et al., 2009; Nagashima et al., 2018; Wheeler et al., 2001). While the overall effect of additional components such as Fe^{3+} on modeled prehnite stability is difficult to assess, they are likely not as significant as for phases such as pumpellyite and epidote since the Fe^{3+} endmember for prehnite is usually estimated to be ~5% (Liou et al., 1983).

Experimental studies show that prehnite and epidote become more enriched in Al with a decrease in oxygen fugacity and an increase in temperature (Liou et al., 1983). It is therefore likely that the prehnite

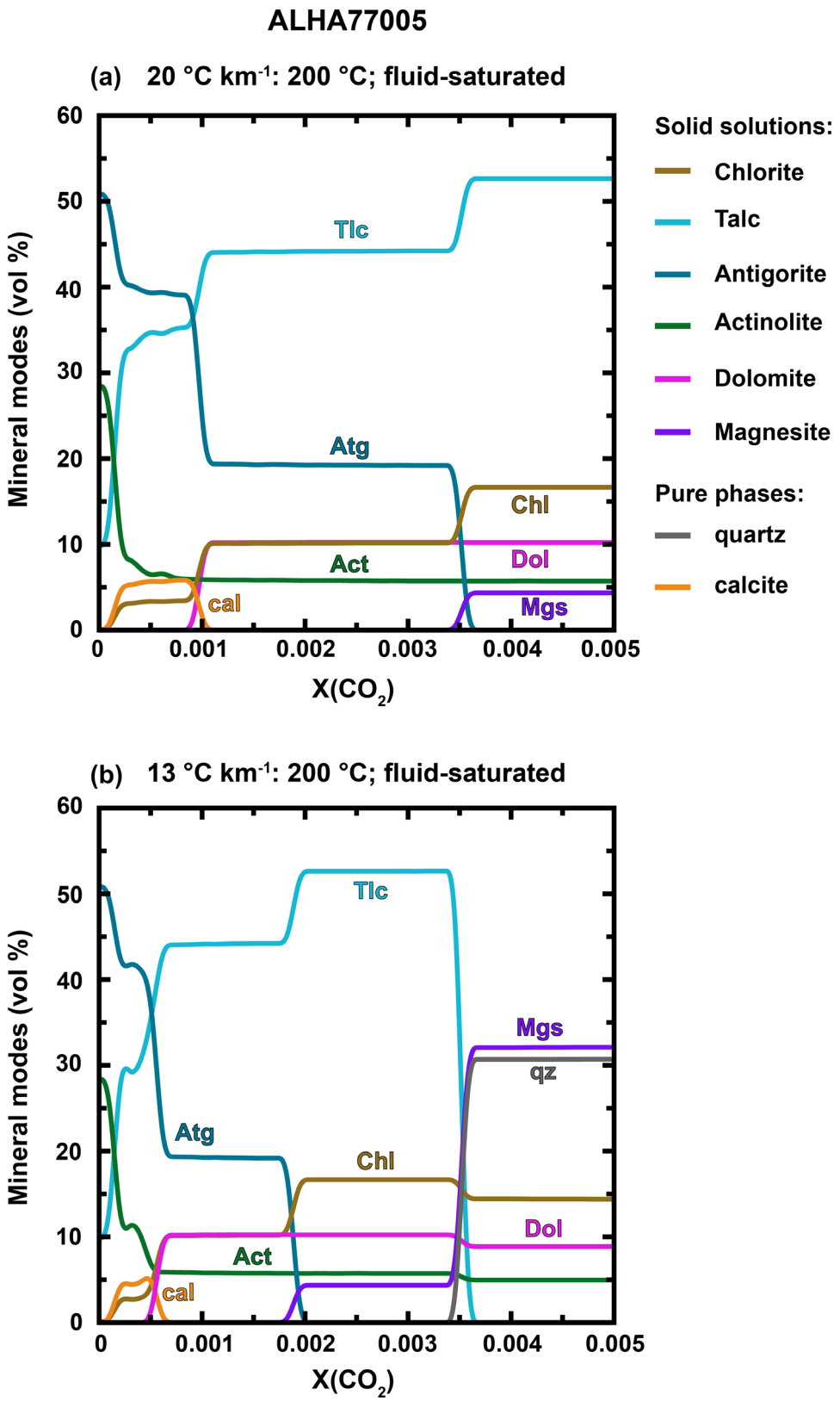

Fig. 5. Modes (vol%) for selected minerals in the ultramafic starting composition of ALHA77005 assuming fluid- and O_2-saturated conditions at 200 °C on the 20 °C km^{-1} (a), and 13 °C km^{-1} (b) geotherms. See Fig. 4 for mineral abbreviations (solid solutions capitalized; pure phases lowercase).

stability in our models in compositions with Fe_2O_3 is underestimated. Since there is likely less Fe^{3+} substitution in prehnite than in pumpellyite, more reducing conditions would likely be more favorable for prehnite stability. Low oxygen fugacities during metamorphism could result in the formation of prehnite instead of pumpellyite, which may explain the absence of pumpellyite detections in spectral studies from orbit. However, the current non-detection of pumpellyite in visible and near-infrared spectra could also be due to its spectrum being similar to Mg-rich chlorite (Ehlmann et al., 2009; Viviano et al., 2013), and pumpellyite may still be present on Mars as suggested by its detection using radiative transfer modeling on OMEGA reflectance spectra (Poulet et al., 2008).

Since the solid solution models for antigorite and talc (Table 1) contain no endmembers with trivalent iron, the ultramafic composition is less sensitive to oxidation state and there are no major changes in mineralogy although minor differences are recorded in mineral stability and abundances (Fig. 4).

Effect of CO_2 on Mineral Stabilities and Implications for Mars

Our calculations show that even small amounts of CO_2 during low-grade metamorphism change the mineralogy significantly. In the modeled basaltic compositions with limited fluid availability, zeolites, prehnite, and pumpellyite are only stable at low CO_2, while epidote is stable at higher amounts of CO_2 together with calcite and dolomite. In the modeled fluid-saturated compositions, Ca-Al silicates are replaced by an assemblage dominated by quartz, calcite, chlorite, and muscovite, which is consistent with studies on Earth, where prehnite and the zeolites stilbite and laumontite form at low XCO_2 from basaltic protoliths (Digel & Gordon, 1995; Thompson, 1971). Epidote and wairakite, however, can be stable at higher CO_2 partial pressure (e.g., Gianelli et al., 1998). In regions on Mars where prehnite has been detected, fluids could therefore not have contained significant amounts of CO_2. This may be due to initially low CO_2 in Martian subsurface fluids that have not been in contact with a CO_2-rich atmosphere. It is also possible that the fluids were in contact with a CO_2-poor or "thin" atmosphere (Manning et al., 2006), although a recalculation of the crustal carbonate abundances that have been detected as pCO_2 (Bridges et al., 2019) is in favor of a "thick" atmosphere model (Manning et al., 2006). Alternatively, prehnite may have formed as a result of CO_2 degassing within a hydrothermal system from hot alkali chloride waters as has been suggested for the formation of hydrothermal prehnite on Earth (Wheeler et al., 2001). Chloride-rich fluids have been proposed for Mars based on minerals in melt inclusions in nakhlite meteorites (Filiberto et al., 2014; Giesting & Filiberto, 2016; McCubbin et al., 2013; Viennet et al., 2020). While residual melts are expected to be enriched in halogens compared to the bulk rocks, degassing at shallow depths may release halogens (e.g., Villemant & Boudon, 1999; Wang et al., 2014) and result in chlorine-rich hydrothermal fluids which could have precipitated the low-grade metamorphic assemblages on Mars (e.g., Filiberto et al., 2014).

The carbonates associated with low-grade metamorphic phases may also have formed at the same pressure–temperature conditions from CO_2-rich fluids before degassing or during periods of higher volcanic activity which could have released magmatic gases and increased the CO_2 in the hydrothermal fluids (e.g., Griffith & Shock, 1995). Alternatively, the carbonates could have formed by later low-temperature alteration either in the shallow subsurface or close to the surface (e.g., Ehlmann, Mustard, Murchie, et al., 2008; Van Berk & Fu, 2011; Van Berk et al., 2011; Viviano et al., 2013). Higher amounts of carbonates could have potentially formed during early Mars and later been partially dissolved by acidic weathering (Ehlmann et al., 2009) or replaced by clays and oxides in the presence of later circumneutral fluids (Bridges et al., 2019; Piercy et al., 2019). Until better constraints on textural and geological relationships are available, it is not possible to determine the specific process most likely for carbonate formation. Once the samples drilled by Mars 2020 Perseverance are returned to Earth, the mineralogical relationships can be compared to our models to better constrain carbonate formation in Jezero crater.

For the ultramafic model compositions, CO_2-enriched fluids result in assemblages dominated by talc–carbonate, and quartz–carbonate replacing serpentine. Studies analyzing Compact Reconnaissance Imaging Spectrometer for Mars mineral spectra have suggested that talc could be associated with carbonates detected in the Nili Fossae area (Brown et al., 2010; Viviano et al., 2013). Based on Earth analogs, the presence of talc likely indicates hydrothermal alteration of olivine-rich rocks (e.g., Bjerga et al., 2015; Brown et al., 2005). The fact that olivine seems to be co-located with the talc–carbonate unit could suggest that the alteration reaction was limited by the availability of either fluids or heat (Brown et al., 2010). Our models suggest that serpentine, olivine, talc, and very small amounts of magnesite could coexist at $\leq$0.33 mol kg^{-1} CO_2 when the amount of fluid is restricted to 5 wt% (Fig. 4) and could, therefore, have formed during a single alteration event. Alternatively, the talc and carbonate assemblage could have formed by subsequent carbonation of serpentine as suggested by Viviano et al. (2013)

implying at least two alteration events with different fluid compositions. Similar processes on small scale could explain the mixed-layer serpentine–talc detected by Curiosity, which were likely transported into Gale crater as sedimentary detritus from ultramafic source rocks (Bristow et al., 2021).

In our models, assemblages dominated by quartz and carbonates are predicted to form from basaltic and ultramafic conditions at $X(CO_2)$ of >0.0005 and >0.0035, respectively (Figs. 3 and 5). The alteration of basaltic and ultramafic rocks by CO_2-bearing fluids at hydrothermal or low-grade metamorphic temperatures (>150 °C) could hence produce silica-rich rocks in the Martian subsurface. Although silica-enriched deposits have been reported by the Curiosity rover at Gale crater (Frydenvang et al., 2017; Morris et al., 2016; Rampe et al., 2017; Yen et al., 2017), by the Spirit rover at Gusev crater (Squyres et al., 2008), and by spectral data from orbit (e.g., Milliken et al., 2008), these are mainly composed of amorphous silica, opaline silica, or tridymite and cristobalite rather than quartz, which is the dominant SiO_2 phase in our models. The differences in mineralogy suggest that the observed deposits formed either during low-temperature (<80 °C), diagenetic conditions (Frydenvang et al., 2017), by hydrothermal activity potentially in a hot spring environment (Ruff & Farmer, 2016; Squyres et al., 2008; Yen et al., 2021), by chemical weathering (Milliken et al., 2008) or, contentiously, as detrital accumulations with volcanic precursors (Morris et al., 2016).

Implications for Habitability

While the temperatures considered in our models are too high for the survival of microbial life, deep, metamorphic fluids could either circulate within the crust and be transported to shallower depths and cooler temperatures or remain trapped in the host rock as they cool. Prerequisites for microbial life are a supply of carbon, hydrogen, nitrogen, oxygen, phosphorus, sulfur, specific micronutrients, and an energy source (Fisk & Giovannoni, 1999). While we have not included N, P, and S in our models, they are usually present in low concentrations in Martian meteorites and soils (Eigenbrode et al., 2018; Filiberto et al., 2019; Franz et al., 2017; Grady et al., 1995; Greenwood et al., 2003; Greenwood & Blake, 2006; Kounaves et al., 2014; Nachon et al., 2017; Stern et al., 2015) and can be released during fluid–rock reactions and transported by hydrothermal fluids (Ehrlich, 1996). Where CO_2-bearing fluids are absent, the carbon required for biomass could have been provided by magmatic carbon in basalts, as reported on the Martian surface and in meteorites (Ming et al., 2014; Sephton et al., 2002; Steele et al., 2012).

Deep subsurface environments are expected to be anoxic and oligotrophic, restricting metabolisms to anaerobic respiration and fermentation (Lovley & Chapelle, 1995). On Earth, subsurface lithoautotrophic microbial ecosystems use a diversity of metabolic mechanisms for energy generation, including H_2 oxidation, methanogenesis, anaerobic methane oxidation, iron and sulfur redox transformation, and nitrate reduction (Nealson et al., 2005; Sar et al., 2019; Stevens & McKinley, 2000). In these environments, the fixation of carbon dioxide is a key metabolic process that drives production. Carbon fixation can be achieved by multiple pathways, including the Wood–Ljungdahl, or reductive acetyl-CoA, pathway (Ragsdale & Pierce, 2008), which has been suggested as one of the earliest metabolisms on Earth (Braakman & Smith, 2012; Fuchs, 2011; Nitschke & Russell, 2013) and is employed by acetogenic bacteria, methanogens, and archaeal sulfate reducers (Smith et al., 2019). Microbes with these metabolisms have been shown to inhabit extreme environments close to the thermodynamic limits of life (Berg, 2011) and could hypothetically survive in the Martian subsurface (Cousins, 2015; Cousins & Crawford, 2011; Nixon et al., 2013).

Acetogens metabolize molecular hydrogen and inorganic carbon (CO_2 or HCO^{3-}) to synthesize acetyl-CoA (Drake et al., 2002; Ljungdahl, 1994; Ragsdale, 1997). Methanogens are archaea that produce methane as a by-product of methanogenesis. There are four known methanogenesis pathways (Sorokin et al., 2017; Vanwonterghem et al., 2016), with the most abundant in environmental studies and distributed taxonomically being hydrogenotrophic methanogenesis (Berghuis et al., 2019; Thauer, 1998), which can conserve energy through the conversion of $H_2 + CO_2$ to methane when using the Wood–Ljungdahl pathway for energy generation (Borrel et al., 2016; Grabarse et al., 2001; Ladapo & Whitman, 1990; Stupperich et al., 1983).

Sulfate-reducing bacteria reverse the Wood–Ljungdahl pathway to generate metabolic energy by coupling the oxidation of acetate to H_2 and CO_2 and using sulfate as a terminal electron acceptor, reducing it to hydrogen sulfide (Schauder et al., 1988; Spormann & Thauer, 1988).

On Earth, molecular hydrogen serves as an energy-rich electron donor for chemolithoautotrophic microbial communities in the subsurface (Nealson et al., 2005; Reith, 2011; Stevens & McKinley, 2000) and could therefore also fuel similar communities on Mars. Possible geogenic hydrogen sources in the Martian subsurface could be radiolysis of water (Lin et al., 2005), friction during seismic events (Kita et al., 1982; Lippmann-Pipke et al., 2011) or at the base of ice sheets (Hirose et al., 2011; Telling et al., 2015), and

serpentinization (Hellevang et al., 2011; Onstott et al., 2019; Schulte et al., 2006; Vance & Melwani Daswani, 2020; Westall et al., 2013). Radiolysis has the potential to yield production rates of H_2 comparable to those on Earth due to the increased porosity space at depth (Dzaugis et al., 2018; Tarnas et al., 2018); this process would also create potential electron acceptors, including sulfate via oxidation of sulfides (Lefticariu et al., 2006; Li et al., 2016), which can create an environment to sustain thermophilic sulfate reducers (Chivian et al., 2008; Lin et al., 2006). Serpentinization also produces H_2, particularly at temperatures of 200–315 °C (McCollom & Bach, 2009). However, a consequence of serpentinization is an increase in pH of the reacted fluids (>9), which can play a role in reducing microbial diversity in terrestrial serpentinization settings (Brazelton et al., 2010; Rempfert et al., 2017; Schrenk et al., 2004). The released geogenic H_2 can either react with aqueous or gaseous carbon or with transition metal sulfide catalysts via Fischer–Tropsch-type reduction to produce methane and a variety of hydrocarbons and organic compounds (Jones et al., 2010; McCollom, 2016; Proskurowski et al., 2008; Sherwood Lollar et al., 2006, 2002). Abiogenically produced methane and hydrocarbons could potentially diffuse upward and be used by heterotrophic microbes, such as anaerobic methane oxidizers (Marlow et al., 2014; Purkamo et al., 2015). Serpentinite-hosted ecosystems and environments enriched in H_2 that have a high pH on Earth are typically dominated by hydrogen-oxidizing microaerophilic *Betaproteobacteria* and anoxic, fermenting *Clostridia*, indicating the viability of these metabolisms under serpentinizing conditions (Brazelton et al., 2010; Itävaara et al., 2011; Moser et al., 2005; Schrenk et al., 2013).

The shallower Martian subsurface, where temperatures are expected in the range of 10–100 °C, could potentially host functional groups shown to occupy neutrophilic and iron-rich environments, such as iron-oxidizing bacteria and archaea, which have been reported to inhabit various terrestrial environments including freshwater (e.g., *Gallionella ferruginea*, *Leptothrix, Sideroxydans*), as well as in marine hydrothermal systems (*Mariprofundus ferrooxydans*; Edwards et al., 2004; Emerson & Moyer, 2010; Emerson et al., 2010). Iron-oxidizing microbes have also been identified (e.g., *Pseudomonas* sp. HerB) at the basalt–ice boundary in lava tube caves using olivine as energy source in low O_2 conditions (Popa et al., 2012).

Under anoxic conditions, anaerobic nitrate-dependent Fe^{2+} oxidation could also have supported subsurface microbial communities in the Martian subsurface at circumneutral pH, provided the presence of carbon and nitrate sources (Chakraborty & Picardal, 2013; Price et al., 2018; Straub & Buchholz-Cleven, 1998). Some species of nitrate-dependent Fe^{2+} oxidizer (*Pseudogulbenkiania* sp. strain 2002 and *Ferroglobus placidus*) are capable of fixing carbon autotrophically from CO_2 and other inorganic sources during nitrate-dependent Fe^{2+} oxidation (Hafenbradl et al., 1996; Weber et al., 2006, 2009) and could therefore inhabit subsurface environments with CO_2-bearing fluids on Mars. Where reduced sulfur compounds are present, sulfur-oxidizing metabolisms could also be viable, either using oxygen (aerobic) or nitrate (microaerophilic or anaerobic) as electron acceptors (Macey et al., 2020).

CONCLUSIONS

Our phase equilibria models using basaltic and ultramafic starting compositions and H_2O-CO_2-bearing fluids show that characteristic low-grade metamorphic minerals such as prehnite, zeolite, and serpentine that have been observed spectrally on Mars are only stable at low CO_2. Higher concentrations of CO_2 will result in assemblages dominated by quartz, calcite, chlorite, and muscovite in the basaltic composition, and by talc–chlorite–dolomite, or magnesite–quartz–chlorite–dolomite assemblages in the ultramafic composition. This could imply that the metamorphic fluids were initially CO_2-poor, or the phases were precipitated after the fluids lost CO_2 by degassing, or carbonates and low-grade metamorphic minerals formed during separate alteration events. Carbonates and talc that have been reported together with metamorphic phases, such as serpentine, could have either formed at similar low-grade metamorphic conditions in the presence of a different, CO_2-bearing, fluid composition in the crust. Alternatively, they could have formed by lower temperature surface or shallow subsurface alteration processes when the initial low-grade metamorphic assemblage was exposed to the CO_2-rich atmosphere.

Acknowledgments—The authors thank Dr. Elizabeth Rampe and an anonymous reviewer for their detailed reviews and comments, which greatly improved the manuscript, and Dr. Gordon Osinski for editorial handling. Profound thanks go to Dr. Michael Macey for his comments on the habitability section. JS and SPS acknowledge funding from Research England Expanding Excellence in England (E3) fund (grant code 124.18).

Data Availability Statement—The data that supports the findings of this study are available in the supplementary material of this article.

Editorial Handling—Dr. Gordon Osinski

REFERENCES

Abramov, O., and Kring, D. A. 2005. Impact-Induced Hydrothermal Activity on Early Mars. *Journal of Geophysical Research: Planets* 110. https://doi.org/10.1029/2005JE002453.

Amador, E. S., Bandfield, J. L., Brazelton, W. J., and Kelley, D. 2017. The Lost City Hydrothermal Field: A Spectroscopic and Astrobiological Analogue for Nili Fossae, Mars. *Astrobiology* 17: 1138–60. https://doi.org/10.1089/ast.2016.1606.

Amador, E. S., Bandfield, J. L., and Thomas, N. H. 2018. A Search for Minerals Associated with Serpentinization Across Mars Using CRISM Spectral Data. *Icarus* 311: 113–34. https://doi.org/10.1016/j.icarus.2018.03.021.

Archer, P. D., Franz, H. B., Sutter, B., Arevalo, R. D., Coll, P., Eigenbrode, J. L., Glavin, D. P. et al. 2014. Abundances and Implications of Volatile-Bearing Species from Evolved Gas Analysis of the Rocknest Aeolian Deposit, Gale Crater, Mars. *Journal of Geophysical Research: Planets* 119: 237–54. https://doi.org/10.1002/2013JE004493.

Archer, P. D., Rampe, E. B., Clark, J. V., Tu, V., Sutter, B., Vaniman, D., Ming, D. W. et al. 2020. Detection of Siderite ($FeCO_3$) in Glen Torridon Samples by the Mars Science Laboratory Rover (Abstract #2709). 51st Lunar and Planetary Science Conference. CD-ROM.

Audouard, J., Poulet, F., Vincendon, M., Milliken, R. E., Jouglet, D., Bibring, J.-P., Gondet, B., and Langevin, Y. 2014. Water in the Martian Regolith from OMEGA/Mars Express. *Journal of Geophysical Research: Planets* 119: 1969–89. https://doi.org/10.1002/2014JE004649.

Bandfield, J. L., Glotch, T. D., and Christensen, P. R. 2003. Spectroscopic Identification of Carbonate Minerals in the Martian Dust. *Science* 301: 1084–7. https://doi.org/10.1126/science.1088054.

Berg, I. A. 2011. Ecological Aspects of the Distribution of Different Autotrophic CO_2 Fixation Pathways. *Applied and Environmental Microbiology* 77: 1925–36. https://doi.org/10.1128/AEM.02473-10.

Berghuis, B. A., Yu, F. B., Schulz, F., Blainey, P. C., Woyke, T., and Quake, S. R. 2019. Hydrogenotrophic Methanogenesis in Archaeal Phylum Verstraetearchaeota Reveals the Shared Ancestry of all Methanogens. *Proceedings of the National Academy of Sciences* 116: 5037–5044. https://doi.org/10.1073/pnas.1815631116.

Bibring, J.-P., Langevin, Y., Mustard, J. F., Poulet, François, Arvidson, R., Gendrin, A., Gondet, B. et al. 2006. Global Mineralogical and Aqueous Mars History Derived from OMEGA/Mars Express Data. *Science* 312: 400–4. https://doi.org/10.1126/science.1122659.

Bishop, J. L., Tirsch, D., Tornabene, L. L., Jaumann, R., McEwen, A. S., McGuire, P. C., Ody, A. et al. 2013. Mineralogy and Morphology of Geologic Units at Libya Montes, Mars: Ancient Aqueously Derived Outcrops, Mafic Flows, Fluvial Features, and Impacts. *Journal of Geophysical Research: Planets* 118: 487–513. https://doi.org/10.1029/2012JE004151.

Bjerga, A., Konopásek, J., and Pedersen, R. B. 2015. Talc-Carbonate Alteration of Ultramafic Rocks Within the Leka Ophiolite Complex, Central Norway. *Lithos* 227: 21–36. https://doi.org/10.1016/j.lithos.2015.03.016.

Borrel, G., Adam, P. S., and Gribaldo, S. 2016. Methanogenesis and the Wood-Ljungdahl Pathway: An Ancient, Versatile, and Fragile Association. *Genome Biology and Evolution* 8: 1706–11. https://doi.org/10.1093/gbe/evw114.

Boynton, W. V., Ming, D. W., Kounaves, S. P., Young, S. M. M., Arvidson, R. E., Hecht, M. H., Hoffman, J. et al. 2009. Evidence for Calcium Carbonate at the Mars Phoenix Landing Site. *Science* 325: 61–4. https://doi.org/10.1126/science.1172768.

Boynton, W. V., Taylor, G. J., Evans, L. G., Reedy, R. C., Starr, R., Janes, D. M., Kerry, K. E. et al. 2007. Concentration of H, Si, Cl, K, Fe, and Th in the Low- and Mid-Latitude Regions of Mars. *Journal of Geophysical Research: Planets* 112: E12S99. https://doi.org/10.1029/2007JE002887.

Braakman, R., and Smith, E. 2012. The Emergence and Early Evolution of Biological Carbon-Fixation. *PLOS Computational Biology* 8: e1002455. https://doi.org/10.1371/journal.pcbi.1002455.

Brazelton, W. J., Ludwig, K. A., Sogin, M. L., Andreishcheva, E. N., Kelley, D. S., Shen, C.-C., Edwards, R. L., and Baross, J. A. 2010. Archaea and Bacteria with Surprising Microdiversity Show Shifts in Dominance Over 1,000-Year Time Scales in Hydrothermal Chimneys. *Proceedings of the National Academy of Sciences* 107: 1612–7. https://doi.org/10.1073/pnas.0905369107.

Bridges, J. C., and Grady, M. M. 2000. Evaporite Mineral Assemblages in the Nakhlite (Martian) Meteorites. *Earth and Planetary Science Letters* 176: 267–79. https://doi.org/10.1016/S0012-821X(00)00019-4.

Bridges, J. C., Hicks, L. J., and Treiman, A. H. 2019. Carbonates on Mars. In *Volatiles in the Martian Crust*, edited by J. Filiberto and S. P. Schwenzer, 89–118. Amsterdam: Elsevier. https://doi.org/10.1016/B978-0-12-804191-8.00005-2.

Bridges, J. C., and Schwenzer, S. P. 2012. The Nakhlite Hydrothermal Brine on Mars. *Earth and Planetary Science Letters* 359–360: 117–23. https://doi.org/10.1016/j.epsl.2012.09.044.

Bridges, J. C., Schwenzer, S. P., Leveille, R., Westall, F., Wiens, R. C., Mangold, N., Bristow, T., Edwards, P., and Berger, G. 2015. Diagenesis and Clay Mineral Formation at Gale Crater, Mars. *Journal of Geophysical Research: Planets* 120: 1–19. https://doi.org/10.1002/2014JE004757.

Bristow, T. F., Grotzinger, J. P., Rampe, E. B., Cuadros, J., Chipera, S. J., Downs, G. W., Fedo, C. M. et al. 2021. Brine-Driven Destruction of Clay Minerals in Gale Crater, Mars. *Science* 373: 198–204. https://doi.org/10.1126/science.abg5449.

Bristow, T. F., Rampe, E. B., Achilles, C. N., Blake, D. F., Chipera, S. J., Craig, P., Crisp, J. A. et al. 2018. Clay Mineral Diversity and Abundance in Sedimentary Rocks of Gale Crater, Mars. *Science Advances* 4: eaar3330. https://doi.org/10.1126/sciadv.aar3330.

Brown, A. J., Hook, S. J., Baldridge, A. M., Crowley, J. K., Bridges, N. T., Thomson, B. J., Marion, G. M., de Souza, F. C. R., and Bishop, J. L. 2010. Hydrothermal Formation of Clay-Carbonate Alteration Assemblages in the Nili Fossae Region of Mars. *Earth and Planetary Science Letters* 297: 174–82. https://doi.org/10.1016/j.epsl.2010.06.018.

Brown, A. J., Viviano, C. E., and Goudge, T. A. 2020. Olivine-Carbonate Mineralogy of the Jezero Crater Region. *Journal of Geophysical Research: Planets* 125: e2019JE006011. https://doi.org/10.1029/2019JE006011.

Brown, A. J., Walter, M. R., and Cudahy, T. J. 2005. Hyperspectral Imaging Spectroscopy of a Mars Analogue Environment at the North Pole Dome, Pilbara Craton, Western Australia. *Australian Journal of Earth Sciences* 52: 353–64. https://doi.org/10.1080/08120090500134530.

Bultel, B., Quantin-Nataf, C., Andréani, M., Clénet, H., and Lozac'h, L. 2015. Deep Alteration Between Hellas and Isidis Basins. *Icarus* 260: 141–60. https://doi.org/10.1016/j.icarus.2015.06.037.

Bultel, B., Viennet, J.-C., Poulet, F., Carter, J., and Werner, S. C. 2019. Detection of Carbonates in Martian Weathering Profiles. *Journal of Geophysical Research: Planets* 124: 989–1007. https://doi.org/10.1029/2018JE005845.

Carter, J., and Poulet, F. 2012. Orbital Identification of Clays and Carbonates in Gusev Crater. *Icarus* 219: 250–3. https://doi.org/10.1016/j.icarus.2012.02.024.

Carter, J., Viviano-Beck, C., Loizeau, D., Bishop, J., and Le Deit, L. 2015. Orbital Detection and Implications of Akaganéite on Mars. *Icarus* 253: 296–310. https://doi.org/10.1016/j.icarus.2015.01.020.

Chakraborty, A., and Picardal, F. 2013. Neutrophilic, Nitrate-Dependent, Fe(II) Oxidation by a Dechloromonas Species. *World Journal of Microbiology and Biotechnology* 29: 617–23. https://doi.org/10.1007/s11274-012-1217-9.

Changela, H. G., and Bridges, J. C. 2011. Alteration Assemblages in the Nakhlites: Variation with Depth on Mars. *Meteoritics & Planetary Science* 45: 1847–67. https://doi.org/10.1111/j.1945-5100.2010.01123.x.

Chivian, D., Brodie, E. L., Alm, E. J., Culley, D. E., Dehal, P. S., DeSantis, T. Z., Gihring, T. M. et al. 2008. Environmental Genomics Reveals a Single-Species Ecosystem Deep Within Earth. *Science* 322: 275–8. https://doi.org/10.1126/science.1155495.

Cho, M., and Liou, J. G. 1987. Prehnite-Pumpellyite to Greenschist Facies Transition in the Karmutsen Metabasites, Vancouver Island, B.C. *Journal of Petrology* 28: 417–43. https://doi.org/10.1093/petrology/28.3.417.

Clifford, S. M. 1993. A Model for the Hydrologic and Climatic Behavior of Water on Mars. *Journal of Geophysical Research: Planets* 98: 10973–1016. https://doi.org/10.1029/93JE00225.

Connolly, J. A. D. 1995. Phase Diagram Methods for Graphitic Rocks and Application to the System $C-O-H-FeO-TiO_2-SiO_2$. *Contributions to Mineralogy and Petrology* 119: 94–116. https://doi.org/10.1007/BF00310720.

Connolly, J. A. D. 2005. Computation of Phase Equilibria by Linear Programming: A Tool for Geodynamic Modeling and Its Application to Subduction Zone Decarbonation. *Earth and Planetary Science Letters* 236: 524–41. https://doi.org/10.1016/j.epsl.2005.04.033.

Costello, L. J., Filiberto, J., Crandall, J. R., Potter-McIntyre, S. L., Schwenzer, S. P., Miller, M. A., Hummer, D. R., Olsson-Francis, K., and Perl, S. 2020. Habitability of Hydrothermal Systems at Jezero and Gusev Craters as Constrained by Hydrothermal Alteration of a Terrestrial Mafic Dike. *Geochemistry* 80: 125613. https://doi.org/10.1016/j.chemer.2020.125613.

Cousins, C. 2015. Volcanogenic Fluvial-Lacustrine Environments in Iceland and Their Utility for Identifying Past Habitability on Mars. *Life* 5: 568–86. https://doi.org/10.3390/life5010568.

Cousins, C. R., and Crawford, I. A. 2011. Volcano-Ice Interaction as a Microbial Habitat on Earth and Mars. *Astrobiology* 11: 695–710. https://doi.org/10.1089/ast.2010.0550.

Crandall, J. R., Filiberto, J., Castle, N., Potter-McIntyre, S. L., Schwenzer, S. P., Olsson-Francis, K., and Perl, S. 2021. Habitability of Martian Noachian Hydrothermal Systems as Constrained by a Terrestrial Analog on the Colorado Plateau. *The Planetary Science Journal* 2: 138. https://doi.org/10.3847/PSJ/ac053e.

Digel, S. D., and Gordon, T. M. 1995. Phase Relations in Metabasites and Pressure-Temperature Conditions at the Prehnite-Pumpellyite to Greenschist Facies Transition, Flin Flin, Manitoba Canada. In *Low-Grade Metamorphism of Mafic Rocks*, edited by P. Schiffman and H. W. Day, 67–80. Boulder, CO: Geological Society of America Special Paper.

Doran, P. T., Wharton, R. A., Des Marais, D. J., and McKay, C. P. 1998. Antarctic Paleolake Sediments and the Search for Extinct Life on Mars. *Journal of Geophysical Research: Planets* 103: 28481–93. https://doi.org/10.1029/98JE01713.

Drake, H. L., Küsel, K., and Matthies, C. 2002. Ecological Consequences of the Phylogenetic and Physiological Diversities of Acetogens. *Antonie van Leeuwenhoek* 81: 203–13. https://doi.org/10.1023/A:1020514617738.

Dzaugis, M., Spivack, A. J., and D'Hondt, S. 2018. Radiolytic H2 Production in Martian Environments. *Astrobiology* 18: 1137–46. https://doi.org/10.1089/ast.2017.1654.

Edwards, C. S., and Ehlmann, B. L. 2015. Carbon Sequestration on Mars. *Geology* 43: 863–6. https://doi.org/10.1130/G36983.1.

Edwards, K. J., Bach, W., McCollom, T. M., and Rogers, D. R. 2004. Neutrophilic Iron-Oxidizing Bacteria in the Ocean: Their Habitats, Diversity, and Roles in Mineral Deposition, Rock Alteration, and Biomass Production in the Deep-Sea. *Geomicrobiology Journal* 21: 393–404. https://doi.org/10.1080/01490450490485863.

Ehlmann, B. L., and Edwards, C. S. 2014. Mineralogy of the Martian Surface. *Annual Review of Earth and Planetary Sciences* 42: 291–315. https://doi.org/10.1146/annurev-earth-060313-055024.

Ehlmann, B. L., Mustard, J. F., Clark, R. N., Swayze, G. A., and Murchie, S. L. 2011. Evidence for Low-Grade Metamorphism, Hydrothermal Alteration, and Diagenesis on Mars from Phyllosilicate Mineral Assemblages. *Clays and Clay Minerals* 59: 359–77. https://doi.org/10.1346/CCMN.2011.0590402.

Ehlmann, B. L., Mustard, J. F., Fassett, C. I., Schon, S. C., Head III, J. W., Des Marais, D. J., Grant, J. A., and Murchie, S. L. 2008. Clay Minerals in Delta Deposits and Organic Preservation Potential on Mars. *Nature Geoscience* 1: 355–8. https://doi.org/10.1038/ngeo207.

Ehlmann, B. L., Mustard, J. F., Murchie, S. L., Poulet, F., Bishop, J. L., Brown, A. J., Calvin, W. M. et al. 2008. Orbital Identification of Carbonate-Bearing Rocks on Mars. *Science* 322: 1828–32. https://doi.org/10.1126/science.1164759.

Ehlmann, B. L., Mustard, J. F., Swayze, G. A., Clark, R. N., Bishop, J. L., Poulet, F., Des Marais, D. J. et al. 2009. Identification of Hydrated Silicate Minerals on Mars Using MRO-CRISM: Geologic Context Near Nili Fossae and Implications for Aqueous Alteration. *Journal of Geophysical Research: Planets* 114: E00D08. https://doi.org/10.1029/2009JE003339.

Ehrlich, H. L. 1996. How Microbes Influence Mineral Growth and Dissolution. *Chemical Geology* 132: 5–9. https://doi.org/10.1016/S0009-2541(96)00035-6.

Eigenbrode, J. L., Summons, R. E., Steele, A., Freissinet, C., Millan, M., Navarro-González, R., Sutter, B. et al. 2018. Organic Matter Preserved in 3-Billion-Year-Old Mudstones at Gale Crater, Mars. *Science* 360: 1096–101. https://doi.org/10.1126/science.aas9185.

Emerson, D., Fleming, E. J., and McBeth, J. M. 2010. Iron-Oxidizing Bacteria: An Environmental and Genomic Perspective. *Annual Review of Microbiology* 64: 561–83. https://doi.org/10.1146/annurev.micro.112408.134208.

Emerson, D., and Moyer, C. L. 2010. Microbiology of Seamounts: Common Patterns Observed in Community Structure. *Oceanography* 23: 148–63.

Feldman, W. C., Prettyman, T. H., Maurice, S., Plaut, J. J., Bish, D. L., Vaniman, D. T., Mellon, M. T. et al. 2004. Global Distribution of Near-Surface Hydrogen on Mars. *Journal of Geophysical Research: Planets* 109. https://doi.org/10.1029/2003JE002160.

Filiberto, J., McCubbin, F. M., and Taylor, G. J. 2019. Volatiles in Martian Magmas and the Interior: Inputs of Volatiles into the Crust and Atmosphere. In *Volatiles in the Martian Crust*, edited by J. Filiberto, and S. P. Schwenzer, 13–33. Elsevier. doi: https://doi.org/10.1016/B978-0-12-804191-8.00002-7.

Filiberto, J., and Schwenzer, S. P. 2013. Alteration mineralogy of Home Plate and Columbia Hills—Formation Conditions in Context to Impact, Volcanism, and Fluvial Activity. *Meteoritics & Planetary Science* 48: 1937–57. https://doi.org/10.1111/maps.12207.

Filiberto, J., Treiman, A. H., Giesting, P. A., Goodrich, C. A., and Gross, J. 2014. High-Temperature Chlorine-Rich Fluid in the Martian Crust: A Precursor to Habitability. *Earth and Planetary Science Letters* 401: 110–5. https://doi.org/10.1016/j.epsl.2014.06.003.

Fisk, M. R., and Giovannoni, S. J. 1999. Sources of Nutrients and Energy for a Deep Biosphere on Mars. *Journal of Geophysical Research: Planets* 104: 11805–15. https://doi.org/10.1029/1999JE900010.

Flahaut, J., Quantin, C., Clenet, H., Allemand, P., Mustard, J. F., and Thomas, P. 2012. Pristine Noachian Crust and Key Geologic Transitions in the Lower Walls of Valles Marineris: Insights into Early Igneous Processes on Mars. *Icarus* 221: 420–35. https://doi.org/10.1016/j.icarus.2011.12.027.

Franz, H. B., McAdam, A. C., Ming, D. W., Freissinet, C., Mahaffy, P. R., Eldridge, D. L., Fischer, W. W. et al. 2017. Large Sulfur Isotope Fractionations in Martian Sediments at Gale Crater. *Nature Geoscience* 10: 658–62. https://doi.org/10.1038/ngeo3002.

Freedman, A. J. E., Bird, D. K., Arnórsson, S., Fridriksson, T., Elders, W. A., and Fridleifsson, G. Ó. 2009. Hydrothermal Minerals Record CO_2 Partial Pressures in the Reykjanes Geothermal System, Iceland. *American Journal of Science* 309: 788–833. https://doi.org/10.2475/09.2009.02.

Frydenvang, J., Gasda, P. J., Hurowitz, J. A., Grotzinger, J. P., Wiens, R. C., Newsom, H. E., Edgett, K. S. et al. 2017. Diagenetic Silica Enrichment and Late-Stage Groundwater Activity in Gale Crater, Mars. *Geophysical Research Letters* 44: 4716–24. https://doi.org/10.1002/2017GL073323.

Fuchs, G. 2011. Alternative Pathways of Carbon Dioxide Fixation: Insights into the Early Evolution of Life? *Annual Review of Microbiology* 65: 631–58. https://doi.org/10.1146/annurev-micro-090110-102801.

Gianelli, G., Mekuria, N., Battaglia, S., Chersicla, A., Garofalo, P., Ruggieri, G., Manganelli, M., and Gebregziabher, Z. 1998. Water-Rock Interaction and Hydrothermal Mineral Equilibria in the Tendaho Geothermal System. *Journal of Volcanology and Geothermal Research* 86: 253–76. https://doi.org/10.1016/S0377-0273(98)00073-0.

Giesting, P. A., and Filiberto, J. 2016. The Formation Environment of Potassic-Chloro-Hastingsite in the Nakhlites MIL 03346 and Pairs and NWA 5790: Insights from Terrestrial Chloro-Amphibole. *Meteoritics & Planetary Science* 51: 2127–53. https://doi.org/10.1111/maps.12675.

Glotch, T. A., and Rogers, A. D. 2013. Evidence for Magma-Carbonate Interaction Beneath Syrtis Major, Mars. *Journal of Geophysical Research: Planets* 118: 126–37. https://doi.org/10.1029/2012JE004230.

Golden, D. C., Ming, D. W., Schwandt, C. S., Lauer, H. V., Socki, R. A., Morris, R. V., Lofgren, G. E., and McKay, G. A. 2001. A Simple Inorganic Process for Formation of Carbonates, Magnetite, and Sulfides in Martian Meteorite ALH84001. *American Mineralogist* 86: 370–5. https://doi.org/10.2138/am-2001-2-321.

Golden, D. C., Ming, D. W., Schwandt, C. S., Morris, R. V., Yang, S. V., and Lofgren, G. E. 2000. An Experimental Study on Kinetically-Driven Precipitation of Calcium-Magnesium-Iron Carbonates from Solution: Implications for the Low-Temperature Formation of Carbonates in Martian Meteorite Allan Hills 84001. *Meteoritics & Planetary Science* 35: 457–65. https://doi.org/10.1111/j.1945-5100.2000.tb01428.x.

Goudge, T. A., Milliken, R. E., Head, J. W., Mustard, J. F., and Fassett, C. I. 2017. Sedimentological Evidence for a Deltaic Origin of the Western Fan Deposit in Jezero Crater, Mars and Implications for Future Exploration. *Earth and Planetary Science Letters* 458: 357–65. https://doi.org/10.1016/j.epsl.2016.10.056.

Goudge, T. A., Mustard, J. F., Head, J. W., Fassett, C. I., and Wiseman, S. M. 2015. Assessing the Mineralogy of the Watershed and Fan Deposits of the Jezero Crater Paleolake System, Mars. *Journal of Geophysical Research: Planets* 120: 775–808. https://doi.org/10.1002/2014JE004782.

Grabarse, W., Mahlert, F., Duin, E. C., Goubeaud, M., Shima, S., Thauer, R. K., Lamzin, V., and Ermler, U. 2001. On the Mechanism of Biological Methane Formation: Structural Evidence for Conformational Changes in Methyl-Coenzyme M Reductase Upon Substrate Binding. *Journal of Molecular Biology* 309: 315–30. https://doi.org/10.1006/jmbi.2001.4647.

Grady, M. M., Wright, I. P., and Pillinger, C. T. 1995. A Search for Nitrates in Martian Meteorites. *Journal of Geophysical Research: Planets* 100: 5449–55. https://doi.org/10.1029/94JE02803.

Greenwood, J. P., and Blake, R. E. 2006. Evidence for an Acidic Ocean on Mars from Phosphorus Geochemistry of Martian Soils and Rocks. *Geology* 34: 953–6. https://doi.org/10.1130/G22415A.1.

Greenwood, J. P., Blake, R. E., and Coath, C. D. 2003. Ion Microprobe Measurements of 18O/16O Ratios of Phosphate Minerals in the Martian Meteorites ALH84001 and Los Angeles. *Geochimica et Cosmochimica Acta* 67: 2289–98. https://doi.org/10.1016/S0016-7037(03)00130-3.

Griffith, L. L., and Shock, E. L. 1995. A Geochemical Model for the Formation of Hydrothermal Carbonates on Mars. *Nature* 377: 406. https://doi.org/10.1038/377406a0.

Griffith, L. L., and Shock, E. L. 1997. Hydrothermal Hydration of Martian Crust: Illustration via Geochemical Model Calculations. *Journal of Geophysical Research: Planets* 102: 9135–43. https://doi.org/10.1029/96JE02939.

Grotzinger, J. P., Arvidson, R. E., Bell, J. F., Calvin, W., Clark, B. C., Fike, D. A., Golombek, M. et al. 2005. Stratigraphy and Sedimentology of a Dry to Wet Eolian Depositional System, Burns Formation, Meridiani Planum, Mars. *Earth and Planetary Science Letters* 240: 11–72. https://doi.org/10.1016/j.epsl.2005.09.039.

Hafenbradl, D., Keller, M., Dirmeier, R., Rachel, R., Roßnagel, P., Burggraf, S., Huber, H., and Stetter, K. O. 1996. Ferroglobus Placidus gen. nov., sp. nov., a Novel Hyperthermophilic Archaeum that Oxidizes Fe^{2+} at Neutral pH Under Anoxic Conditions. *Archives of Microbiology* 166: 308–14. https://doi.org/10.1007/s002030050388.

Halevy, I., Fischer, W. W., and Eiler, J. M. 2011. Carbonates in the Martian Meteorite Allan Hills 84001 Formed at 18 ± 4 °C in a Near-Surface Aqueous Environment. *Proceedings of the National Academy of Sciences* 108:16895–9. https://doi.org/10.1073/pnas.1109444108.

Harvey, R. P., and McSween, H. Y. 1996. A Possible High-Temperature Origin for the Carbonates in the Martian Meteorite ALH84001. *Nature* 382: 49–51. https://doi.org/10.1038/382049a0.

Hellevang, H., Huang, S., and Thorseth, I. H. 2011. The Potential for Low-Temperature Abiotic Hydrogen Generation and a Hydrogen-Driven Deep Biosphere. *Astrobiology* 11: 711–24. https://doi.org/10.1089/ast.2010.0559.

Herd, C. D. K. 2003. The Oxygen Fugacity of Olivine-Phyric Martian Basalts and the Components Within the Mantle and Crust of Mars. *Meteoritics & Planetary Science* 38: 1793–805. https://doi.org/10.1111/j.1945-5100.2003.tb00015.x.

Herd, C. D. K. 2006. Insights into the Redox History of the NWA 1068/1110 Martian Basalt from Mineral Equilibria and Vanadium Oxybarometry. *American Mineralogist* 91: 1616–27. https://doi.org/10.2138/am.2006.2104.

Hicks, L. J., Bridges, J. C., and Gurman, S. J. 2014. Ferric Saponite and Serpentine in the Nakhlite Martian Meteorites. *Geochimica et Cosmochimica Acta* 136: 194–210. https://doi.org/10.1016/j.gca.2014.04.010.

Hirose, T., Kawagucci, S., and Suzuki, K. 2011. Mechanoradical H2 Generation During Simulated Faulting: Implications for an Earthquake-Driven Subsurface Biosphere. *Geophysical Research Letters* 38. https://doi.org/10.1029/2011GL048850.

Holland, T., and Powell, R. 1991. A Compensated-Redlich-Kwong (CORK) Equation for Volumes and Fugacities of CO_2 and H_2O in the Range 1 bar to 50 kbar and 100–1600°C. *Contributions to Mineralogy and Petrology* 109: 265–73. https://doi.org/10.1007/BF00306484.

Holland, T., and Powell, R. 1996. Thermodynamics of order-disorder in minerals: II. Symmetric formalism applied to solid solutions. *American Mineralogist* 81: 1425–37.

Holland, T. J. B., and Powell, R. 1998. An Internally Consistent Thermodynamic Data Set for Phases of Petrological Interest. *Journal of Metamorphic Geology* 16: 309–43.

Holland, T. J. B., and Powell, R. 2011. An Improved and Extended Internally Consistent Thermodynamic Dataset for Phases of Petrological Interest, Involving a New Equation of State for Solids. *Journal of Metamorphic Geology* 29: 333–83. https://doi.org/10.1111/j.1525-1314.2010.00923.x.

Horgan, B. H. N., Anderson, R. B., Dromart, G., Amador, E. S., and Rice, M. S. 2020. The Mineral Diversity of Jezero Crater: Evidence for Possible Lacustrine Carbonates on Mars. *Icarus* 339: 113526. https://doi.org/10.1016/j.icarus.2019.113526.

Hu, R., Kass, D. M., Ehlmann, B. L., and Yung, Y. L. 2015. Tracing the Fate of Carbon and the Atmospheric Evolution of Mars. *Nature Communications* 6: 1–9. https://doi.org/10.1038/ncomms10003.

Itävaara, M., Nyyssönen, M., Kapanen, A., Nousiainen, A., Ahonen, L., and Kukkonen, I. 2011. Characterization of Bacterial Diversity to a Depth of 1500 m in the Outokumpu Deep Borehole, Fennoscandian Shield. *FEMS Microbiology Ecology* 77: 295–309. https://doi.org/10.1111/j.1574-6941.2011.01111.x.

Jain, N., and Chauhan, P. 2015. Study of Phyllosilicates and Carbonates from the Capri Chasma Region of Valles Marineris on Mars Based on Mars Reconnaissance Orbiter-Compact Reconnaissance Imaging Spectrometer for Mars (MRO-CRISM) Observations. *Icarus* 250: 7–17. https://doi.org/10.1016/j.icarus.2014.11.018.

Jolliff, B. L., Mittlefehldt, D. W., Farrand, W. H., Knoll, A. H., McLennan, S. M., and Gellert, R. 2019. Mars Exploration Rover Opportunity: Water and Other Volatiles on Ancient Mars. In *Volatiles in the Martian Crust*, edited by J. Filiberto and S. P. Schwenzer, 285–328. Amsterdam: Elsevier. https://doi.org/10.1016/B978-0-12-804191-8.00010-6.

Jones, E. G., Lineweaver, C. H., and Clarke, J. D. 2011. An Extensive Phase Space for the Potential Martian Biosphere. *Astrobiology* 11: 1017–33. https://doi.org/10.1089/ast.2011.0660.

Jones, L. C., Rosenbauer, R., Goldsmith, J. I., and Oze, C. 2010. Carbonate Control of H2 and CH4 Production in Serpentinization Systems at Elevated P-Ts. *Geophysical Research Letters* 37. https://doi.org/10.1029/2010GL043769.

Kita, I., Matsuo, S., and Wakita, H. 1982. H_2 Generation by Reaction Between H_2O and Crushed Rock: An Experimental Study on H_2 Degassing from the Active Fault Zone. *Journal of Geophysical Research: Solid Earth* 87: 10789–95. https://doi.org/10.1029/JB087iB13p10789.

Kounaves, S. P., Carrier, B. L., O'Neil, G. D., Stroble, S. T., and Claire, M. W. 2014. Evidence of Martian Perchlorate, Chlorate, and Nitrate in Mars Meteorite EETA79001: Implications for Oxidants and Organics. *Icarus* 229: 206–13. https://doi.org/10.1016/j.icarus.2013.11.012.

Kounaves, S. P., and Oberlin, E. A. 2019. Volatiles Measured by the Phoenix Lander at the Northern Plains of Mars. In *Volatiles in the Martian Crust*, edited by J. Filiberto and S. P. Schwenzer, 265–83. Amsterdam: Elsevier. https://doi.org/10.1016/B978-0-12-804191-8.00009-X.

Ladapo, J., and Whitman, W. B. 1990. Method for Isolation of Auxotrophs in the Methanogenic Archaebacteria: Role of the Acetyl-CoA Pathway of Autotrophic CO_2 Fixation in *Methanococcus maripaludis*. *Proceedings of the National Academy of Sciences* 87: 5598–602. https://doi.org/10.1073/pnas.87.15.5598.

Lasue, J., Clifford, S. M., Conway, S. J., Mangold, N., and Butcher, F. E. G. 2019. The Hydrology of Mars Including a Potential Cryosphere. In *Volatiles in the Martian Crust*, edited by J. Filiberto and S. P. Schwenzer, 185–246. Amsterdam: Elsevier. https://doi.org/10.1016/B978-0-12-804191-8.00007-6.

Lefticariu, L., Pratt, L. M., and Ripley, E. M. 2006. Mineralogic and Sulfur Isotopic Effects Accompanying Oxidation of Pyrite in Millimolar Solutions of Hydrogen Peroxide at Temperatures from 4 to 150°C. *Geochimica et Cosmochimica Acta* 70: 4889–905. https://doi.org/10.1016/j.gca.2006.07.026.

Leshin, L. A., Mahaffy, P. R., Webster, C. R., Cabane, M., Coll, P., Conrad, P. G., Archer, P. D. et al. 2013. Volatile, Isotope, and Organic Analysis of Martian Fines with the Mars Curiosity Rover. *Science* 341. https://doi.org/10.1126/science.1238937.

Li, L., Wing, B. A., Bui, T. H., McDermott, J. M., Slater, G. F., Wei, S., Lacrampe-Couloume, G., and Lollar, B. S. 2016. Sulfur Mass-Independent Fractionation in Subsurface Fracture Waters Indicates a Long-Standing Sulfur Cycle in Precambrian rocks. *Nature Communications* 7: 13252. https://doi.org/10.1038/ncomms13252.

Lin, L.-H., Hall, J., Lippmann-Pipke, J., Ward, J. A., Lollar, B. S., DeFlaun, M., Rothmel, R. et al. 2005. Radiolytic H_2 in Continental Crust: Nuclear Power for Deep Subsurface Microbial Communities. *Geochemistry, Geophysics, Geosystems* 6: https://doi.org/10.1029/2004GC000907.

Lin, L.-H., Wang, P.-L., Rumble, D., Lippmann-Pipke, J., Boice, E., Pratt, L. M., Lollar, B. S. et al. 2006. Long-Term Sustainability of a High-Energy, Low-Diversity Crustal Biome. *Science* 314: 479–82. https://doi.org/10.1126/science.1127376.

Liou, J. G., Kim, H. S., and Maruyama, S. 1983. Prehnite—Epidote Equilibria and Their Petrologic Applications. *Journal of Petrology* 24: 321–42. https://doi.org/10.1093/petrology/24.4.321.

Lippmann-Pipke, J., Erzinger, J., Zimmer, M., Kujawa, C., Boettcher, M., Heerden, E. V., Bester, A., Moller, H., Stroncik, N. A., and Reches, Z. 2011. Geogas Transport in Fractured Hard Rock—Correlations with Mining Seismicity at 3.54 km Depth, TauTona Gold Mine, South Africa. *Applied Geochemistry* 26: 2134–46. https://doi.org/10.1016/j.apgeochem.2011.07.011.

Litvak, M. L., Mitrofanov, I. G., Hardgrove, C., Stack, K. M., Sanin, A. B., Lisov, D., Boynton, W. V. et al. 2016. Hydrogen and Chlorine Abundances in the Kimberley Formation of Gale Crater Measured by the DAN Instrument on Board the Mars Science Laboratory Curiosity Rover. *Journal of Geophysical Research: Planets* 121: 836–45. https://doi.org/10.1002/2015JE004960.

Ljungdahl, L. G. 1994. The Acetyl-CoA Pathway and the Chemiosmotic Generation of ATP During Acetogenesis. In *Acetogenesis*, edited by H. L. Drake, 63–87. Boston, MA: Springer US. https://doi.org/10.1007/978-1-4615-1777-1_2.

Lodders, K. 1998. A Survey of Shergottite, Nakhlite and Chassigny Meteorites Whole-Rock Compositions. *Meteoritics & Planetary Science* 33: A183–90. https://doi.org/10.1111/j.1945-5100.1998.tb01331.x.

Lovley, D. R., and Chapelle, F. H. 1995. Deep Subsurface Microbial Processes. *Reviews of Geophysics* 33: 365–81. https://doi.org/10.1029/95RG01305.

Macey, M. C., Fox-Powell, M., Ramkissoon, N. K., Stephens, B. P., Barton, T., Schwenzer, S. P., Pearson, V. K., Cousins, C. R., and Olsson-Francis, K. 2020. The Identification of Sulfide Oxidation as a Potential Metabolism Driving Primary Production on Late Noachian Mars. *Scientific Reports* 10: 10941. https://doi.org/10.1038/s41598-020-67815-8.

Manning, C. V., McKay, C. P., and Zahnle, K. J. 2006. Thick and Thin Models of the Evolution of Carbon Dioxide on Mars. *Icarus* 180: 38–59. https://doi.org/10.1016/j.icarus.2005.08.014.

Marlow, J. J., LaRowe, D. E., Ehlmann, B. L., Amend, J. P., and Orphan, V. J. 2014. The Potential for Biologically Catalyzed Anaerobic Methane Oxidation on Ancient Mars. *Astrobiology* 14: 292–307. https://doi.org/10.1089/ast.2013.1078.

Massonne, H.-J., and Willner, A. P. 2008. Phase Relations and Dehydration Behaviour of Psammopelite and Mid-Ocean Ridge Basalt at Very-Low-Grade to Low-Grade Metamorphic Conditions. *European Journal of Mineralogy* 867–879: https://doi.org/10.1127/0935-1221/2008/0020-1871.

Maurice, S., Feldman, W., Diez, B., Gasnault, O., Lawrence, D. J., Pathare, A., and Prettyman, T. 2011. Mars Odyssey Neutron Data: 1. Data Processing and Models of Water-Equivalent-Hydrogen Distribution. *Journal of Geophysical Research: Planets* 116. https://doi.org/10.1029/2011JE003810.

McCollom, T. M. 2016. Abiotic Methane Formation During Experimental Serpentinization of Olivine. *Proceedings of the National Academy of Sciences* 113: 13965–70. https://doi.org/10.1073/pnas.1611843113.

McCollom, T. M., and Bach, W. 2009. Thermodynamic Constraints on Hydrogen Generation During Serpentinization of Ultramafic Rocks. *Geochimica et Cosmochimica Acta* 73: 856–75. https://doi.org/10.1016/j.gca.2008.10.032.

McCubbin, F. M., Elardo, S. M., Shearer, C. K., Smirnov, A., Hauri, E. H., and Draper, D. S. 2013. A Petrogenetic Model for the Comagmatic Origin of Chassignites and Nakhlites: Inferences from Chlorine-Rich Minerals, Petrology, and Geochemistry. *Meteoritics & Planetary Science* 48: 819–53. https://doi.org/10.1111/maps.12095.

McGovern, P. J., Solomon, S. C., Smith, D. E., Zuber, M. T., Simons, M., Wieczorek, M. A., Phillips, R. J. et al. 2004. Correction to "Localized Gravity/Topography Admittance and Correlation Spectra on Mars: Implications for Regional and Global Evolution". *Journal of Geophysical Research: Planets* 109: E07007.

McGovern, P. J., Solomon, S. C., Smith, D. E., Zuber, M. T., Simons, M., Wieczorek, M. A., Phillips, R. J., Neumann, G. A., Aharonson, O., and Head, J. W. 2002. Localized Gravity/Topography Admittance and Correlation Spectra on Mars: Implications for Regional and Global Evolution. *Journal of Geophysical Research: Planets* 107:19-1–19–25. https://doi.org/10.1029/2002JE001854.

McMahon, S., O'Malley-James, J., and Parnell, J. 2013. Circumstellar Habitable Zones for Deep Terrestrial Biospheres. *Planetary and Space Science* 85: 312–8. https://doi.org/10.1016/j.pss.2013.07.002.

McSween, H. Y., Labotka, T. C., and Viviano-Beck, C. E. 2015. Metamorphism in the Martian Crust. *Meteoritics & Planetary Science* 50: 590–603. https://doi.org/10.1111/maps.12330.

Melwani Daswani, M., Schwenzer, S. P., Reed, M. H., Wright, I. P., and Grady, M. M. 2016. Alteration Minerals, Fluids, and Gases on Early Mars: Predictions from 1-D Flow Geochemical Modeling of Mineral Assemblages in Meteorite ALH 84001. *Meteoritics & Planetary Science* 51: 2154–74. https://doi.org/10.1111/maps.12713.

Michalski, J. R., Cuadros, J., Niles, P. B., Parnell, J., Rogers, A. D., and Wright, S. P. 2013. Groundwater Activity on

Mars and Implications for a Deep Biosphere. *Nature Geoscience* 6: 133–8. https://doi.org/10.1038/ngeo1706.

Michalski, J. R., and Niles, P. B. 2010. Deep Crustal Carbonate Rocks Exposed by Meteor Impact on Mars. *Nature Geoscience* 3: 751–5. https://doi.org/10.1038/ngeo971.

Milliken, R. E., Mustard, J. F., Poulet, F., Jouglet, D., Bibring, J.-P., Gondet, B., and Langevin, Y. 2007. Hydration State of the Martian Surface as Seen by Mars Express OMEGA: 2. H_2O Content of the Surface. *Journal of Geophysical Research: Planets* 112. https://doi.org/10.1029/2006JE002853.

Milliken, R. E., Swayze, G. A., Arvidson, R. E., Bishop, J. L., Clark, R. N., Ehlmann, B. L., Green, R. O. et al. 2008. Opaline Silica in Young Deposits on Mars. *Geology* 36: 847–50. https://doi.org/10.1130/G24967A.1.

Ming, D. W., Archer, P. D., Glavin, D. P., Eigenbrode, J. L., Franz, H. B., Sutter, B., Brunner, A. E. et al. 2014. Volatile and Organic Compositions of Sedimentary Rocks in Yellowknife Bay, Gale Crater, Mars. *Science* 343: 1245267. https://doi.org/10.1126/science.1245267.

Mitrofanov, I. G., Litvak, M. L., Sanin, A. B., Starr, R. D., Lisov, D. I., Kuzmin, R. O., Behar, A. et al. 2014. Water and Chlorine Content in the Martian Soil Along the First 1900 m of the Curiosity Rover Traverse as Estimated by the DAN Instrument. *Journal of Geophysical Research: Planets* 119: 1579–96. https://doi.org/10.1002/2013JE004553.

Mittlefehldt, D. W. 1994. ALH84001, a Cumulate Orthopyroxenite Member of the Martian Meteorite Clan. *Meteoritics* 29: 214–21. https://doi.org/10.1111/j.1945-5100.1994.tb00673.x.

Mittlefehldt, D. W., Gellert, R., Ming, D. W., and Yen, A. S. 2019. Alteration Processes in Gusev Crater, Mars: Volatile/Mobile Element Contents of Rocks and Soils Determined by the Spirit Rover. In *Volatiles in the Martian Crust*, edited by J. Filiberto and S. P. Schwenzer, 329–68. Amsterdam: Elsevier. https://doi.org/10.1016/B978-0-12-804191-8.00011-8.

Möller, P., Weise, S. M., Althaus, E., Bach, W., Behr, H. J., Borchardt, R., Bräuer, K. et al. 1997. Paleofluids and Recent Fluids in the Upper Continental Crust: Results from the German Continental Deep Drilling Program (KTB). *Journal of Geophysical Research: Solid Earth* 102: 18233–54. https://doi.org/10.1029/96JB02899.

Morris, R. V., Ruff, S. W., Gellert, R., Ming, D. W., Arvidson, R. E., Clark, B. C., Golden, D. C. et al. 2010. Identification of Carbonate-Rich Outcrops on Mars by the Spirit Rover. *Science* 329: 421–4. https://doi.org/10.1126/science.1189667.

Morris, R. V., Vaniman, D. T., Blake, D. F., Gellert, R., Chipera, S. J., Rampe, E. B., Ming, D. W. et al. 2016. Silicic Volcanism on Mars Evidenced by Tridymite in High-SiO_2 Sedimentary Rock at Gale Crater. *Proceedings of the National Academy of Sciences* 113: 7071–6. https://doi.org/10.1073/pnas.1607098113.

Moser, D. P., Gihring, T. M., Brockman, F. J., Fredrickson, J. K., Balkwill, D. L., Dollhopf, M. E., Lollar, B. S. et al. 2005. Desulfotomaculum and Methanobacterium spp. Dominate a 4- to 5-Kilometer-Deep Fault. *Applied and Environmental Microbiology* 71: 8773–83. https://doi.org/10.1128/AEM.71.12.8773-8783.2005.

Mustard, J. F. 2019. Sequestration of Volatiles in the Martian Crust Through Hydrated Minerals: A Significant Planetary Reservoir of Water. In *Volatiles in the Martian Crust*, edited by J. Filiberto and S. P. Schwenzer, 247–63. Amsterdam: Elsevier. https://doi.org/10.1016/B978-0-12-804191-8.00008-8.

Mustard, J. F., Murchie, S. L., Pelkey, S. M., Ehlmann, B. L., Milliken, R. E., Grant, J. A., Bibring, J.-P. et al. 2008. Hydrated Silicate Minerals on Mars Observed by the Mars Reconnaissance Orbiter CRISM Instrument. *Nature* 454: 305–9. https://doi.org/10.1038/nature07097.

Nachon, M., Mangold, N., Forni, O., Kah, L. C., Cousin, A., Wiens, R. C., Anderson, R. et al. 2017. Chemistry of Diagenetic Features Analyzed by ChemCam at Pahrump Hills, Gale Crater, Mars. *Icarus* 281: 121–36. https://doi.org/10.1016/j.icarus.2016.08.026.

Nagashima, M., Iwasa, K., and Akasaka, M. 2018. Crystal Chemistry and Oxidation State of Fe-Rich Prehnite from a Hydrothermally Altered Dolerite. *Mineralogy and Petrology* 112: 173–84. https://doi.org/10.1007/s00710-017-0530-2.

Nealson, K. H., Inagaki, F., and Takai, K. 2005. Hydrogen-Driven Subsurface Lithoautotrophic Microbial Ecosystems (SLiMEs): Do They Exist and Why Should We Care? *Trends in Microbiology* 13: 405–10. https://doi.org/10.1016/j.tim.2005.07.010.

Newton, R. C., Charlu, T. V., and Kleppa, O. J. 1980. Thermochemistry of the High Structural State Plagioclases. *Geochimica et Cosmochimica Acta* 44: 933–41.

Niles, P. B., Catling, D. C., Berger, G., Chassefière, E., Ehlmann, B. L., Michalski, J. R., Morris, R., Ruff, S. W., and Sutter, B. 2013. Geochemistry of Carbonates on Mars: Implications for Climate History and Nature of Aqueous Environments. *Space Science Reviews* 174: 301–28. https://doi.org/10.1007/s11214-012-9940-y.

Nitschke, W., and Russell, M. J. 2013. Beating the Acetyl Coenzyme A-Pathway to the Origin of Life. *Philosophical Transactions of the Royal Society B: Biological Sciences* 368: 20120258. https://doi.org/10.1098/rstb.2012.0258.

Nixon, S. L., Cousins, C. R., and Cockell, C. S. 2013. Plausible Microbial Metabolisms on Mars. *Astronomy & Geophysics* 54: 1.13–1.16. https://doi.org/10.1093/astrogeo/ats034.

Nurmi, P. A., Kukkonen, I. T., and Lahermo, P. W. 1988. Geochemistry and Origin of Saline Groundwaters in the Fennoscandian Shield. *Applied Geochemistry* 3: 185–203. https://doi.org/10.1016/0883-2927(88)90007-8.

Onstott, T. C., Ehlmann, B. L., Sapers, H., Coleman, M., Ivarsson, M., Marlow, J. J., Neubeck, A., and Niles, P. 2019. Paleo-Rock-Hosted Life on Earth and the Search on Mars: A Review and Strategy for Exploration. *Astrobiology* 19: 1230–62. https://doi.org/10.1089/ast.2018.1960.

Padrón-Navarta, J. A., Sánchez-Vizcaíno, V. L., Hermann, J., Connolly, J. A. D., Garrido, C. J., Gómez-Pugnaire, M. T., and Marchesi, C. 2013. Tschermak's Substitution in Antigorite and Consequences for Phase Relations and Water Liberation in High-Grade Serpentinites. *Lithos* 178: 186–96. https://doi.org/10.1016/j.lithos.2013.02.001.

Parro, L. M., Jiménez-Díaz, A., Mansilla, F., and Ruiz, J. 2017. Present-Day Heat Flow Model of Mars. *Scientific Reports* 7: 45629. https://doi.org/10.1038/srep45629.

Piercy, J. D., Bridges, J. C., and Hicks, L. J. 2019. Carbonates Within Lafayette. 82nd Annual Meeting of the Meteoritical Society #6408. p. 1.

Plesa, A.-C., Grott, M., Tosi, N., Breuer, D., Spohn, T., and Wieczorek, M. A. 2016. How Large Are Present-Day Heat

Flux Variations Across the Surface of Mars? *Journal of Geophysical Research: Planets* 121: 2386–403. https://doi.org/10.1002/2016JE005126.

Popa, R., Smith, A. R., Popa, R., Boone, J., and Fisk, M. 2012. Olivine-Respiring Bacteria Isolated from the Rock-Ice Interface in a Lava-Tube Cave, a Mars Analog Environment. *Astrobiology* 12: 9–18. https://doi.org/10.1089/ast.2011.0639.

Poulet, F., Mangold, N., Loizeau, D., Bibring, J.-P., Langevin, Y., Michalski, J., and Gondet, B. 2008. Abundance of Minerals in the Phyllosilicate-Rich Units on Mars. *Astronomy & Astrophysics* 487: L41–4. https://doi.org/10.1051/0004-6361:200810150.

Price, A., Pearson, V. K., Schwenzer, S. P., Miot, J., and Olsson-Francis, K. 2018. Nitrate-Dependent Iron Oxidation: A Potential Mars Metabolism. *Frontiers in Microbiology* 9: 513. https://doi.org/10.3389/fmicb.2018.00513.

Proskurowski, G., Lilley, M. D., Seewald, J. S., Früh-Green, G. L., Olson, E. J., Lupton, J. E., Sylva, S. P., and Kelley, D. S. 2008. Abiogenic Hydrocarbon Production at Lost City Hydrothermal Field. *Science* 319: 604–7. https://doi.org/10.1126/science.1151194.

Purkamo, L., Bomberg, M., Nyyssönen, M., Kukkonen, I., Ahonen, L., and Itävaara, M. 2015. Heterotrophic Communities Supplied by Ancient Organic Carbon Predominate in Deep Fennoscandian Bedrock Fluids. *Microbial Ecology* 69: 319–32. https://doi.org/10.1007/s00248-014-0490-6.

Ragsdale, S. W. 1997. The Eastern and Western Branches of the Wood/Ljungdahl Pathway: How the East and West Were Won. *BioFactors* 6: 3–11. https://doi.org/10.1002/biof.5520060102.

Ragsdale, S. W., and Pierce, E. 2008. Acetogenesis and the Wood–Ljungdahl Pathway of CO_2 Fixation. *Biochimica et Biophysica Acta (BBA)—Proteins and Proteomics* 1784: 1873–98. https://doi.org/10.1016/j.bbapap.2008.08.012.

Rampe, E. B., Blake, D. F., Bristow, T. F., Ming, D. W., Vaniman, D. T., Morris, R. V., Achilles, C. N. et al. 2020. Mineralogy and Geochemistry of Sedimentary Rocks and Eolian Sediments in Gale Crater, Mars: A Review After Six Earth Years of Exploration with Curiosity. *Geochemistry* 80: 125605. https://doi.org/10.1016/j.chemer.2020.125605.

Rampe, E. B., Ming, D. W., Blake, D. F., Bristow, T. F., Chipera, S. J., Grotzinger, J. P., Morris, R. V. et al. 2017. Mineralogy of an Ancient Lacustrine Mudstone Succession from the Murray Formation, Gale Crater, Mars. *Earth and Planetary Science Letters* 471: 172–85. https://doi.org/10.1016/j.epsl.2017.04.021.

Reith, F. 2011. Life in the Deep Subsurface. *Geology* 39: 287–8. https://doi.org/10.1130/focus032011.1.

Rempfert, K. R., Miller, H. M., Bompard, N., Nothaft, D., Matter, J. M., Kelemen, P., Fierer, N., and Templeton, A. S. 2017. Geological and Geochemical Controls on Subsurface Microbial Life in the Samail Ophiolite, Oman. *Frontiers in Microbiology* 8: 56. https://doi.org/10.3389/fmicb.2017.00056.

Ruff, S. W., and Farmer, J. D. 2016. Silica deposits on Mars with Features Resembling Hot Spring Biosignatures at El Tatio in Chile. *Nature Communications* 7: 1–10. https://doi.org/10.1038/ncomms13554.

Ruff, S. W., Niles, P. B., Alfano, F., and Clarke, A. B. 2014. Evidence for a Noachian-Aged Ephemeral Lake in Gusev Crater, Mars. *Geology* 42: 359–62. https://doi.org/10.1130/G35508.1.

Salvatore, M. R., Goudge, T. A., Bramble, M. S., Edwards, C. S., Bandfield, J. L., Amador, E. S., Mustard, J. F., and Christensen, P. R. 2018. Bulk Mineralogy of the NE Syrtis and Jezero Crater Regions of Mars Derived Through Thermal Infrared Spectral Analyses. *Icarus* 301: 76–96. https://doi.org/10.1016/j.icarus.2017.09.019.

Sar, P., Dutta, A., Bose, H., Mandal, S., and Kazy, S. K. 2019. Deep Biosphere: Microbiome of the Deep Terrestrial Subsurface. In *Microbial Diversity in Ecosystem Sustainability and Biotechnological Applications: Volume 1. Microbial Diversity in Normal & Extreme Environments*, edited by T. Satyanarayana, B. N. Johri, and S. K. Das, 225–65. Singapore: Springer. https://doi.org/10.1007/978-981-13-8315-1_8.

Sautter, V., Jambon, A., and Boudouma, O. 2006. Cl-Amphibole in the Nakhlite MIL 03346: Evidence for Sediment Contamination in a Martian Meteorite. *Earth and Planetary Science Letters* 252: 45–55. https://doi.org/10.1016/j.epsl.2006.09.024.

Schauder, R., Preuß, A., Jetten, M., and Fuchs, G. 1988. Oxidative and Reductive Acetyl CoA/Carbon Monoxide Dehydrogenase Pathway in *Desulfobacterium autotrophicum*. *Archives of Microbiology* 151: 84–9. https://doi.org/10.1007/BF00444674.

Schmidt, M. E., Schrader, C. M., and McCoy, T. J. 2013. The Primary fO_2 of Basalts Examined by the Spirit Rover in Gusev Crater, Mars: Evidence for Multiple Redox States in the Martian Interior. *Earth and Planetary Science Letters* 384: 198–208. https://doi.org/10.1016/j.epsl.2013.10.005.

Schrenk, M. O., Brazelton, W. J., and Lang, S. Q. 2013. Serpentinization, Carbon, and Deep Life. *Reviews in Mineralogy and Geochemistry* 75: 575–606. https://doi.org/10.2138/rmg.2013.75.18.

Schrenk, M. O., Kelley, D. S., Bolton, S. A., and Baross, J. A. 2004. Low Archaeal Diversity Linked to Subseafloor Geochemical Processes at the Lost City Hydrothermal Field, Mid-Atlantic Ridge. *Environmental Microbiology* 6: 1086–95. https://doi.org/10.1111/j.1462-2920.2004.00650.x.

Schulte, M., Blake, D., Hoehler, T., and McCollom, T. 2006. Serpentinization and Its Implications for Life on the Early Earth and Mars. *Astrobiology* 6: 364–76. https://doi.org/10.1089/ast.2006.6.364.

Schwenzer, S. P., and Kring, D. A. 2013. Alteration Minerals in Impact-Generated Hydrothermal Systems—Exploring Host Rock Variability. *Icarus* 226: 487–96. https://doi.org/10.1016/j.icarus.2013.06.003.

Semprich, J., and Filiberto, J. 2020. High-Pressure Metamorphic Mineralogy of the Martian Crust with Implications for Density and Seismic Profiles. *Meteoritics & Planetary Science* 55: 1600–14. https://doi.org/10.1111/maps.13535.

Semprich, J., Schwenzer, S. P., Treiman, A. H., and Filiberto, J. 2019. Phase Equilibria Modeling of Low-Grade Metamorphic Martian Rocks. *Journal of Geophysical Research: Planets* 124: 681–702. https://doi.org/10.1029/2018JE005869.

Sephton, M. A., Wright, I. P., Gilmour, I., de Leeuw, J. W., Grady, M. M., and Pillinger, C. T. 2002. High Molecular Weight Organic Matter in Martian Meteorites. *Planetary and Space Science* 50: 711–6. https://doi.org/10.1016/S0032-0633(02)00053-3.

Sherwood Lollar, B., Lacrampe-Couloume, G., Slater, G. F., Ward, J., Moser, D. P., Gihring, T. M., Lin, L.-H., and Onstott, T. C. 2006. Unravelling Abiogenic and Biogenic Sources of Methane in the Earth's Deep Subsurface. *Chemical Geology* 226: 328–39. https://doi.org/10.1016/j.chemgeo.2005.09.027.

Sherwood Lollar, B., Westgate, T. D., Ward, J. A., Slater, G. F., and Lacrampe-Couloume, G. 2002. Abiogenic Formation of Alkanes in the Earth's Crust as a Minor Source for Global Hydrocarbon Reservoirs. *Nature* 416: 522–4. https://doi.org/10.1038/416522a.

Smith, A. R., Kieft, B., Mueller, R., Fisk, M. R., Mason, O. U., Popa, R., and Colwell, F. S. 2019. Carbon Fixation and Energy Metabolisms of a Subseafloor Olivine Biofilm. *The ISME Journal* 13: 1737–49. https://doi.org/10.1038/s41396-019-0385-0.

Sohl, F., Schubert, G., and Spohn, T. 2005. Geophysical Constraints on the Composition and Structure of the Martian Interior. *Journal of Geophysical Research: Planets* 110: E12008. https://doi.org/10.1029/2005JE002520.

Sorokin, D. Y., Makarova, K. S., Abbas, B., Ferrer, M., Golyshin, P. N., Galinski, E. A., Ciordia, S. et al. 2017. Discovery of Extremely Halophilic, Methyl-Reducing Euryarchaea Provides Insights into the Evolutionary Origin of Methanogenesis. *Nature Microbiology* 2: 1–11. https://doi.org/10.1038/nmicrobiol.2017.81.

Spormann, A. M., and Thauer, R. K. 1988. Anaerobic Acetate Oxidation to CO_2 by *Desulfotomaculum acetoxidans*. *Archives of Microbiology* 150: 374–80. https://doi.org/10.1007/BF00408310.

Squyres, S. W., Arvidson, R. E., Ruff, S., Gellert, R., Morris, R. V., Ming, D. W., Crumpler, L. et al. 2008. Detection of Silica-Rich Deposits on Mars. *Science* 320: 1063–7. https://doi.org/10.1126/science.1155429.

Starkey, R. J., and Frost, B. R. 1990. Low-Grade Metamorphism of the Karmutsen Volcanics, Vancouver Island, British Columbia. *Journal of Petrology* 31: 167–95. https://doi.org/10.1093/petrology/31.1.167.

Steele, A., McCubbin, F. M., Fries, M., Kater, L., Boctor, N. Z., Fogel, M. L., Conrad, P. G. et al. 2012. A Reduced Organic Carbon Component in Martian Basalts. *Science* 337: 212–5. https://doi.org/10.1126/science.1220715.

Stern, J. C., Sutter, B., Freissinet, C., Navarro-González, R., McKay, C. P., Archer, P. D., Buch, A. et al. 2015. Evidence for Indigenous Nitrogen in Sedimentary and Aeolian Deposits from the Curiosity Rover Investigations at Gale Crater, Mars. *Proceedings of the National Academy of Sciences* 112: 4245–50. https://doi.org/10.1073/pnas.1420932112.

Stern, J. C., Sutter, B., Archer, P. D., Eigenbrode, J. L., McAdam, A. C., Franz, H. B., Knudson, C. et al. 2018. Major Volatiles Evolved From Eolian Materials in Gale Crater. *Geophysical Research Letters* 45: 10240–8. https://doi.org/10.1029/2018GL079059.

Stevens, T. O., and McKinley, J. P. 2000. Abiotic Controls on H_2 Production from Basalt−Water Reactions and Implications for Aquifer Biogeochemistry. *Environmental Science & Technology* 34: 826–31. https://doi.org/10.1021/es990583g.

Straub, K. L., and Buchholz-Cleven, B. E. E. 1998. Enumeration and Detection of Anaerobic Ferrous Iron-Oxidizing, Nitrate-Reducing Bacteria from Diverse European Sediments. *Applied and Environmental Microbiology* 64: 4846–56. https://doi.org/10.1128/AEM.64.12.4846-4856.1998.

Stupperich, E., Hammel, K. E., Fuchs, G., and Thauer, R. K. 1983. Carbon Monoxide Fixation into the Carboxyl Group of Acetyl Coenzyme A During Autotrophic Growth of Methanobacterium. *FEBS Letters* 152: 21–3. https://doi.org/10.1016/0014-5793(83)80473-6.

Sun, V. Z., and Milliken, R. E. 2015. Ancient and Recent Clay Formation on Mars as Revealed from a Global Survey of Hydrous Minerals in Crater Central Peaks. *Journal of Geophysical Research: Planets* 120: 2293–332. https://doi.org/10.1002/2015JE004918.

Sutter, B., Boynton, W. V., Ming, D. W., Niles, P. B., Morris, R. V., Golden, D. C., Lauer, H. V., Fellows, C., Hamara, D. K., and Mertzman, S. A. 2012. The Detection of Carbonate in the Martian Soil at the Phoenix Landing Site: A Laboratory Investigation and Comparison with the Thermal and Evolved Gas Analyzer (TEGA) Data. *Icarus* 218: 290–6. https://doi.org/10.1016/j.icarus.2011.12.002.

Sutter, B., McAdam, A. C., and Mahaffy, P. R. 2019. Volatile Detections in Gale Crater Sediment and Sedimentary Rock: Results from the Mars Science Laboratory's Sample Analysis at Mars Instrument. In *Volatiles in the Martian Crust*, edited by J. Filiberto and S. P. Schwenzer, 369–92. Amsterdam: Elsevier. https://doi.org/10.1016/B978-0-12-804191-8.00012-X.

Sutter, B., McAdam, A. C., Mahaffy, P. R., Ming, D. W., Edgett, K. S., Rampe, E. B., Eigenbrode, J. L. et al. 2017. Evolved Gas Analyses of Sedimentary Rocks and Eolian Sediment in Gale Crater, Mars: Results of the Curiosity Rover's Sample Analysis at Mars Instrument from Yellowknife Bay to the Namib Dune. *Journal of Geophysical Research: Planets* 122: 2574–609. https://doi.org/10.1002/2016JE005225.

Tajčmanová, L., Connolly, J. A. D., and Cesare, B. 2009. A Thermodynamic Model for Titanium and Ferric Iron Solution in Biotite. *Journal of Metamorphic Geology* 27: 153–65. https://doi.org/10.1111/j.1525-1314.2009.00812.x.

Takai, K., Nakamura, K., Toki, T., Tsunogai, U., Miyazaki, M., Miyazaki, J., Hirayama, H. et al. 2008. Cell Proliferation at 122°C and Isotopically heavy CH_4 Production by a Hyperthermophilic Methanogen Under High-Pressure Cultivation. *Proceedings of the National Academy of Sciences* 105: 10949–54. https://doi.org/10.1073/pnas.0712334105.

Tarnas, J. D., Mustard, J. F., Sherwood, L. B., Bramble, M. S., Cannon, K. M., Palumbo, A. M., and Plesa, A.-C. 2018. Radiolytic H_2 Production on Noachian Mars: Implications for Habitability and Atmospheric Warming. *Earth and Planetary Science Letters* 502: 133–45. https://doi.org/10.1016/j.epsl.2018.09.001.

Telling, J., Boyd, E. S., Bone, N., Jones, E. L., Tranter, M., MacFarlane, J. W., Martin, P. G. et al. 2015. Rock Comminution as a Source of Hydrogen for Subglacial Ecosystems. *Nature Geoscience* 8: 851–5. https://doi.org/10.1038/ngeo2533.

Thauer, R. K. 1998. Biochemistry of Methanogenesis: A Tribute to Marjory Stephenson: 1998 Marjory Stephenson Prize Lecture. *Microbiology* 144: 2377–406. https://doi.org/10.1099/00221287-144-9-2377.

Thomas, N. H., Ehlmann, B. L., Rapin, W., Rivera-Hernández, F., Stein, N. T., Frydenvang, J., Gabriel, T. et al. 2020. Hydrogen Variability in the Murray Formation, Gale Crater, Mars. *Journal of Geophysical Research: Planets* 125. https://doi.org/10.1029/2019je006289.

Thomas, N. H., and Bandfield, J. L. 2017. Identification and Refinement of Martian Surface Mineralogy Using Factor

Analysis and Target Transformation of Near-Infrared Spectroscopic Data. *Icarus* 291: 124–35. https://doi.org/10.1016/j.icarus.2017.03.001.

Thompson, A. B. 1971. P CO_2 in Low-Grade Metamorphism; Zeolite, Carbonate, Clay Mineral, Prehnite Relations in the System CaO-Al_2O3-SiO_2-CO_2-H_2O. *Contributions to Mineralogy and Petrology* 33: 145–61. https://doi.org/10.1007/BF00386112.

Thompson, J. B., and Waldbaum, D. R. 1969. Mixing Properties of Sanidine Crystalline Solutions: III. Calculations Based on Two-Phase Data. *American Mineralogist* 54: 811–38.

Travis, B. J., Rosenberg, N. D., and Cuzzi, J. N. 2003. On the Role of Widespread Subsurface Convection in Bringing Liquid Water Close to Mars' Surface. *Journal of Geophysical Research: Planets* 108: https://doi.org/10.1029/2002JE001877.

Tu, V. M., Rampe, E. B., Bristow, T. F., Thorpe, M. T., Clark, J. V., Castle, N., Fraeman, A. A. et al. 2021. A Review of the Phyllosilicates in Gale Crater as Detected by the CheMin Instrument on the Mars Science Laboratory, Curiosity Rover. *Minerals* 11: 847. https://doi.org/10.3390/min11080847.

Turner, S. M. R., Bridges, J. C., Grebby, S., and Ehlmann, B. L. 2016. Hydrothermal Activity Recorded in Post Noachian-Aged Impact Craters on Mars. *Journal of Geophysical Research: Planets* 121: 608–25. https://doi.org/10.1002/2015JE004989.

Valley, J. W., Eiler, J. M., Graham, C. M., Gibson, E. K., Romanek, C. S., and Stolper, E. M. 1997. Low-Temperature Carbonate Concretions in the Martian Meteorite ALH84001: Evidence from Stable Isotopes and Mineralogy. *Science* 275: 1633–8. https://doi.org/10.1126/science.275.5306.1633.

Van Berk, W., and Fu, Y. 2011. Reproducing Hydrogeochemical Conditions Triggering the Formation of Carbonate and Phyllosilicate Alteration Mineral Assemblages on Mars (Nili Fossae Region). *Journal of Geophysical Research: Planets* 116. https://doi.org/10.1029/2011JE003886.

Van Berk, W., Ilger, J.-M., Fu, Y., and Hansen, C. 2011. Decreasing CO2 Partial Pressure Triggered Mg–Fe–Ca Carbonate Formation in Ancient Martian Crust Preserved in the ALH84001 Meteorite. *Geofluids* 11: 6–17. https://doi.org/10.1111/j.1468-8123.2010.00296.x.

Vance, S. D., and Melwani Daswani, M. 2020. Serpentinite and the Search for Life Beyond Earth. *Philosophical Transactions of the Royal Society A: Mathematical, Physical and Engineering Sciences* 378: 20180421. https://doi.org/10.1098/rsta.2018.0421.

Vanwonterghem, I., Evans, P. N., Parks, D. H., Jensen, P. D., Woodcroft, B. J., Hugenholtz, P., and Tyson, G. W. 2016. Methylotrophic Methanogenesis Discovered in the Archaeal Phylum Verstraetearchaeota. *Nature Microbiology* 1: 1–9. https://doi.org/10.1038/nmicrobiol.2016.170.

Viennet, J.-C., Bernard, S., Le Guillou, C., Sautter, V., Schmitt-Kopplin, P., Beyssac, O., Pont, S. et al. 2020. Tardi-Magmatic Precipitation of Martian Fe/Mg-Rich Clay Minerals via Igneous Differentiation. *Geochemical Perspectives Letters* 47–52. https://doi.org/10.7185/geochemlet.2023.

Villemant, B., and Boudon, G. 1999. H_2O and Halogen (F, Cl, Br) Behaviour During Shallow Magma Degassing Processes. *Earth and Planetary Science Letters* 168: 271–86. https://doi.org/10.1016/S0012-821X(99)00058-8.

Viviano, C. E., Moersch, J. E., and McSween, H. Y. 2013. Implications for Early Hydrothermal Environments on Mars Through the Spectral Evidence for Carbonation and Chloritization Reactions in the Nili Fossae Region. *Journal of Geophysical Research: Planets* 118: 1858–72. https://doi.org/10.1002/jgre.20141.

Wang, L.-X., Marks, M. A. W., Keller, J., and Markl, G. 2014. Halogen Variations in Alkaline Rocks from the Upper Rhine Graben (SW Germany): Insights into F, Cl and Br Behavior During Magmatic Processes. *Chemical Geology* 380: 133–44. https://doi.org/10.1016/j.chemgeo.2014.05.003.

Weber, K. A., Hedrick, D. B., Peacock, A. D., Thrash, J. C., White, D. C., Achenbach, L. A., and Coates, J. D. 2009. Physiological and Taxonomic Description of the Novel Autotrophic, Metal Oxidizing Bacterium, Pseudogulbenkiania sp. Strain 2002. *Applied Microbiology and Biotechnology* 83: 555–65. https://doi.org/10.1007/s00253-009-1934-7.

Weber, K. A., Pollock, J., Cole, K. A., O'Connor, S. M., Achenbach, L. A., and Coates, J. D. 2006. Anaerobic Nitrate-Dependent Iron(II) Bio-Oxidation by a Novel Lithoautotrophic Betaproteobacterium, Strain 2002. *Applied and Environmental Microbiology* 72: 686–94. https://doi.org/10.1128/AEM.72.1.686-694.2006.

Wernicke, L. J., and Jakosky, B. M. 2021. Martian Hydrated Minerals: A Significant Water Sink. *Journal of Geophysical Research: Planets* 126: e2019JE006351. https://doi.org/10.1029/2019JE006351.

Westall, F., Loizeau, D., Foucher, F., Bost, N., Betrand, M., Vago, J., and Kminek, G. 2013. Habitability on Mars from a Microbial Point of View. *Astrobiology* 13: 887–97. https://doi.org/10.1089/ast.2013.1000.

Wheeler, R. S., Browne, P. R. L., and Rodgers, K. A. 2001. Iron-Rich and Iron-Poor Prehnites from the Way Linggo Epithermal Au-Ag Deposit, Southwest Sumatra, and the Heber Geothermal Field, California. *Mineralogical Magazine* 65: 397–406. https://doi.org/10.1180/002646101300119475.

White, R. W., Powell, R., Holland, T. J. B., and Worley, B. A. 2000. The Effect of TiO_2 and Fe_2O_3 on Metapelitic Assemblages at Greenschist and Amphibolite Facies Conditions: Mineral Equilibria Calculations in the System K_2O–FeO–MgO–Al_2O_3–SiO_2–H_2O–TiO_2–Fe_2O_3. *Journal of Metamorphic Geology* 18: 497–511. https://doi.org/10.1046/j.1525-1314.2000.00269.x.

White, R. W., Powell, R., Holland, T. J. B., Johnson, T. E., and Green, E. C. R. 2014. New Mineral Activity-Composition Relations for Thermodynamic Calculations in Metapelitic Systems. *Journal of Metamorphic Geology* 32: 261–86. https://doi.org/10.1111/jmg.12071.

Wray, J. J., Murchie, S. L., Bishop, J. L., Ehlmann, B. L., Milliken, R. E., Wilhelm, M. B., Seelos, K. D., and Chojnacki, M. 2016. Orbital Evidence for More Widespread Carbonate-Bearing Rocks on Mars. *Journal of Geophysical Research: Planets* 121: 652–77. https://doi.org/10.1002/2015JE004972.

Yen, A. S., Ming, D. W., Vaniman, D. T., Gellert, R., Blake, D. F., Morris, R. V., Morrison, S. M. et al. 2017. Multiple Stages of Aqueous Alteration Along Fractures in Mudstone and Sandstone Strata in Gale Crater, Mars. *Earth and Planetary Science Letters* 471: 186–98. https://doi.org/10.1016/j.epsl.2017.04.033.

Yen, A. S., Morris, R. V., Ming, D. W., Schwenzer, S. P., Sutter, B., Vaniman, D. T., Treiman, A. H. et al. 2021.

Formation of Tridymite and Evidence for a Hydrothermal History at Gale Crater, Mars. *Journal of Geophysical Research: Planets* 126: e2020JE006569: https://doi.org/10.1029/2020JE006569.

Zipfel, J., Schröder, C., Jolliff, B. L., Gellert, R., Herkenhoff, K. E., Rieder, R., Anderson, R. et al. 2011. Bounce Rock—A Shergottite-Like Basalt Encountered at Meridiani Planum, Mars. *Meteoritics & Planetary Science* 46: 1–20. https://doi.org/10.1111/j.1945-5100.2010.01127.x.

Zolotov, M. Y., and Mironenko, M. V. 2016. Chemical Models for Martian Weathering Profiles: Insights into Formation of Layered Phyllosilicate and Sulfate Deposits. *Icarus* 275: 203–20. https://doi.org/10.1016/j.icarus.2016.04.011.

SUPPORTING INFORMATION

Additional supporting information may be found in the online version of this article.

Table S1. Mineral modes in vol% calculated for Bounce Rock and the ultramafic composition ALHA77005 for different oxidation states (red = reduced with FeO only; ox = oxidized with 10% Fe_2O_3), geotherms (20 = 20 °C km^{-1}; 13 = 13 °C km^{-1}), and fluid content (5 wt% with variable H_2O-CO_2 except for fluid saturated). Values listed in each sheet correspond to the figure specified in row 2.